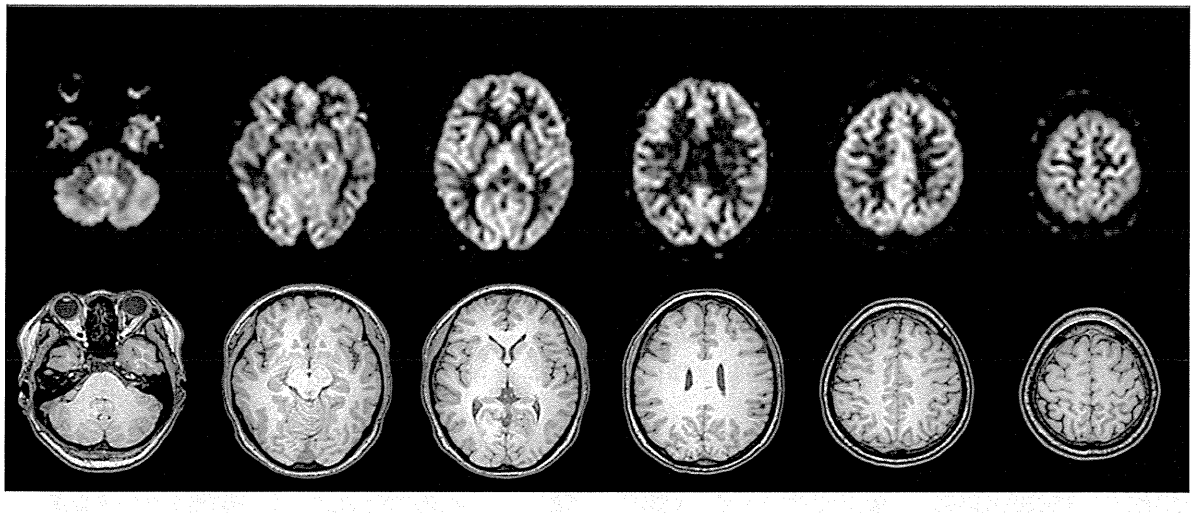

Fig. 1. The upper row showed the typical example of ASL CBF maps acquired in a single healthy volunteer, and lower row showed corresponding slices of T1-weighted image.

data sets were analyzed using QBrain®1.1 [22]. The volume quantifications were first performed with manual segmentation and second with the fully automatic segmentation algorithms. Using the software, the T2-hyperintense lesions can be reliably quantified in the milliliter range.

2.5. Measure of whole brain volume

We regarded the gray matter volume plus white matter volume as the whole brain volume. The values of gray and white matter volumes of individual subjects were extracted with the Easy Volume toolbox [29] running on Matlab 7.0. The gray matter and white matter volume images were derived from the segmented 3D-T1 image calculated using SPM5.

2.6. Statistical analysis

We first evaluated the correlations among the EDSS score, age, duration of illness and the ratio of T2-hyperintense lesion volume/whole brain volume in the MS patients by using Pearson's correlation analysis. Statistical analyses were performed using SPSS Statistics for Windows 17.0 software (SPSS, Tokyo, Japan).

Next, statistical analyses for the CBF were performed using SPM5 software. We evaluated the difference in regional CBF (rCBF) between the MS patients and healthy subjects using age and gender as nuisance variables. Only correlations that met the following criteria were deemed statistically significant: seed levels of $P < .05$ [false discovery rate (FDR) corrected] and a cluster level of $P < .05$ (uncorrected).

Next, correlations between rCBF values and the ratio of T2-hyperintense lesion volume/whole brain volume and between rCBF values and EDSS scores were assessed using age, gender and duration of illness as nuisance variables. Only correlations that met the following criteria were deemed significant: a seed level of $P < .001$ (uncorrected) and a cluster level of $P < .05$ (uncorrected).

Finally, we highlighted the influence of the T2-hyperintense lesion on the CBF. We masked the latter results with the regions for which the results of the former analysis were regarded as significant.

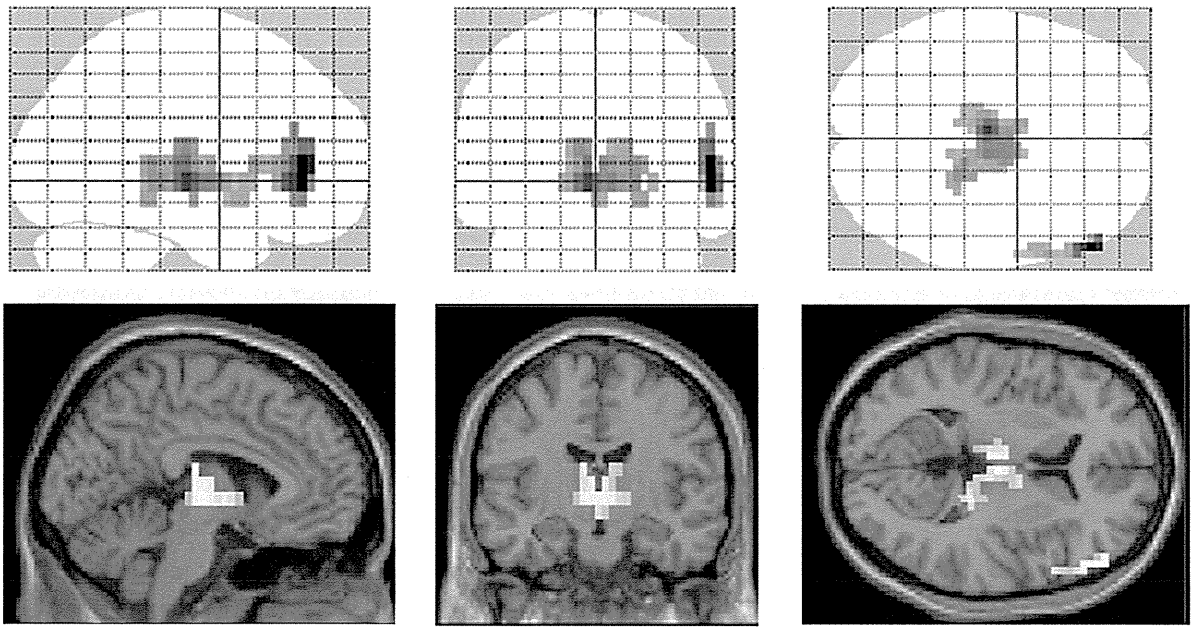

Fig. 2. There were significant reductions of CBF in the right prefrontal cortex and bilateral thalami in the MS patients compared to the healthy controls [$P < .05$ (FDR corrected)].

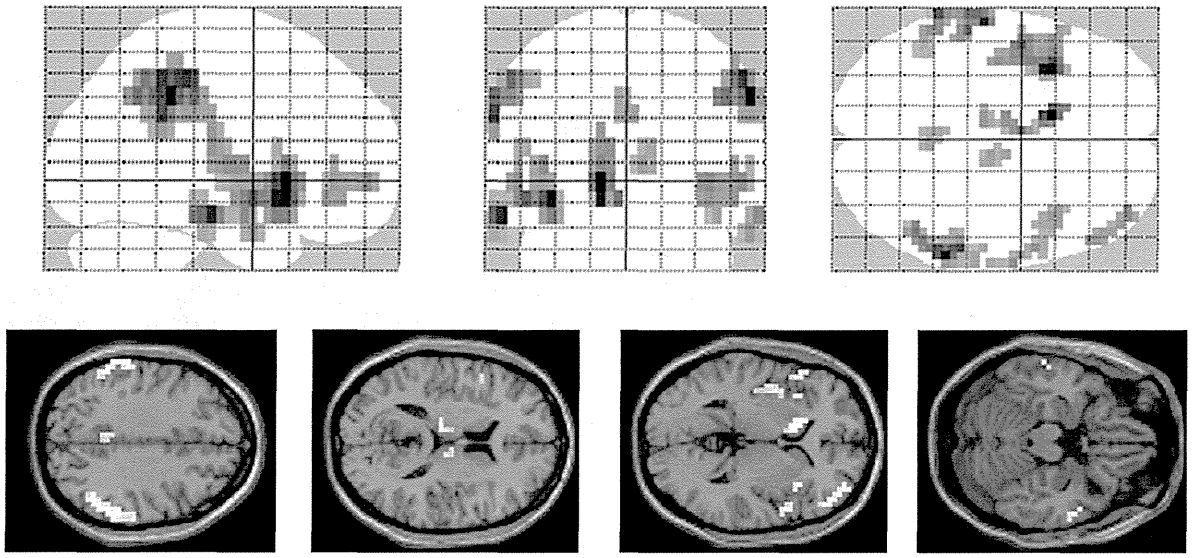

Fig. 3. There were negative correlations between the T2-hyperintense lesion volume/whole brain volume ratio and the regional CBF values in several areas throughout the brain in the MS patients ($P < .001$, uncorrected).

This mask was based on partially the same data of the latter analysis; there existed a multiple testing problem. So, we use the formal thresholding (e.g., FDR) that accounts for this multiplicity [30]. The mask applied the seed levels of $P < .05$ (FDR corrected) as statistically significant.

3. Results

There were no significant correlations between any combinations of two factors of EDSS score, age, duration of illness and the ratio of T2-hyperintense lesion volume/whole brain volume in the MS patients (data not shown). There were significant reductions of CBF in the bilateral thalami and right frontal region of the MS patients compared to the healthy controls (Fig. 2 and Table 2).

There was no increase of CBF in MS patients (data not shown). In the MS patient group, the T2-hyperintense lesion volume/whole brain volume ratio was negatively correlated with rCBF values in the right frontal region, both parietal and temporal regions, both insulae, the left caudate, both thalami and both posterior cinguli (Fig. 3 and Table 3). There were no differences of regional CBF between relapsing–remitting MS patients and secondary progressive MS patients (data not shown).

In contrast, there was no correlation between the EDSS scores and rCBF values (data not shown). There were significant negative correlations between the ratio of the T2-hyperintense lesion volume to whole brain volume and CBF in both thalami when we masked the second results with the regions in which the results of the first analysis were regarded as significant (Fig. 4).

4. Discussion

To our knowledge, this is the first evaluation of the possible relationships between clinical presentations of MS and CBF using pCASL. By using the pCASL technique, we found significant correlations between the volume of T2-hyperintense lesions and the rCBF values. In particular, CBF in the thalamus was significantly decreased in the patients with MS compared to that of the healthy subjects, and thalamic CBF was correlated with the volume of T2-hyperintense lesion.

There were a few studies of MS using CASL and PASL [14,31]. One study using the CASL showed the reduction of thalamic CBF in MS; however, they did not evaluate the correlation between the volume of T2-hyperintense lesions and the rCBF values [14]. On the other hand, the study using PASL showed not the correlation between them but the correlation between the volume of lesions and mean cortical CBF [31]. These facts may indicate that the CBF study using pCASL calculates the rigorous CBF value. In addition, these studies, including our study, did not show the correlation between the EDSS and rCBF. This may result from the fact that the EDSS mainly focused on the ambulatory ability, not on the higher brain function, so the change of

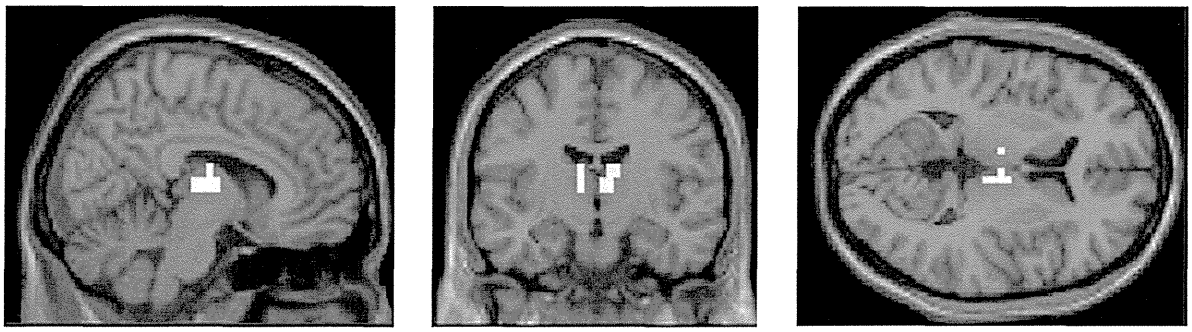

Fig. 4. When the correlation analysis was restricted in both thalami where the CBF reduction was detected in the MS patients, there were significant negative correlations between the T2-hyperintense lesion volume/whole brain volume ratio and the CBF values.

cortical CBF in MS did not reflect the EDSS score. In recent years, the MS Functional Composite (MSFC) was proposed for a new multidimensional clinical outcome measure of MS [32]. The MSFC comprises quantitative functional measures of three key clinical dimensions of MS: leg function ambulation, arm/hand function and cognitive function. Further studies with information on MSFC are necessary to address this issue. Additionally, we showed the CBF reduction of the patients with MS in the inferior prefrontal cortex. Previous study showed that MS patients with long duration of disease showed atrophy of the thalami and inferior frontal gyrus [33]. The participants in this study showed relatively long disease duration (Table 1); then the CBF of the patients would show the reduction.

We also found negative correlations between the ratio of the T2-hyperintense lesion volume/whole brain volume and regional CBF in several areas throughout the brain in the MS patients. We focused on volume and not on distribution of the T2-hyperintense lesion in the whole brain, and therefore, the relationship between the volume of lesion and the regional CBF was not examined. However, some previous studies showed reduced metabolism in the prefrontal, parietal and occipital cortex and hippocampus, thalamus, putamen and caudate in MS [7,8,13,14], and those findings are compatible with our results.

Regarding the thalamus, an MRI study of MS patients reported a decrease in thalamic volume and *N*-acetyl aspartate [34]. Those authors also identified the thalamic neuronal loss in MS patients by postmortem examination. Evaluations of the metabolism and perfusion in the brains of patients with MS have also revealed hypometabolism and hypoperfusion in the thalamus [9,12,14] Furthermore, PET metabolic studies suggest a possible correlation between thalamic hypometabolism and cognitive impairment [7], memory disturbance [13] and the volume of deep white matter lesions [8]. The decreased thalamic CBF observed in our study is consistent with the findings of these previous studies. Another study using diffusion tensor imaging revealed the fine neural networks in the CNS [35]. The thalamus is regarded as the central relay station of the brain, and the reciprocal influence between the thalamus and its associated areas has been well described [36]. The decreased CBF that we observed in the thalamus of the MS patients may be an indication of a disconnection between cortical regions and subcortical relay systems due to the lesion process in MS.

There were some limitations of this study. First, we dealt with the whole brain CBF images, including the gray matter and white matter, voxel-basically. However, we could not detect the white matter CBF change. Previous study showed that the female patients with MS showed the change of white matter compared with men, while gender did not impact gray matter atrophy [33]. Along with the dissemination of MS lesions in space and time, co-gender participants may influence on our results. Further work with single-gender MS patients will be necessary to confirm our results. Second, we did not classify the participants into the three subgroups of MS. The subgroups of MS were defined by the clinical course of illness, and this is not for a cross-sectional study containing the first episode of illness. Not only our study but also two previous cross-sectional studies using ASL also did not show the differences among the subgroups of MS [14,31]. Further longitudinal work would show the difference among the subgroups. A third limitation of the present study is that we did not eliminate the effect of immunomodulating treatment on CBF. Further work with drug-free MS patients will be necessary to confirm our results.

In conclusion, our findings indicate that the noninvasive pCASL is a useful technique which demonstrated that regional CBF values are closely related to the brain lesions in MS. In addition, our results suggest that the demyelinating lesions in MS mainly have a remote effect on the function of the thalamus. Measurement of CBF by pCASL MRI has the potential to be an objective marker for monitoring disease activity in MS (Tables 2 and 3).

Table 2
Regions that showed significant differences in cerebral blood flow between the patients with multiple sclerosis ($n = 27$) and healthy controls ($n = 24$) using age and gender as nuisance variables.

Cluster size	*Z* score	*x*	*y*	*z*	Brain region
35	5.17	56	40	8	Right frontal lobe
114	4.61	−4	−16	0	Left thalamus
	4	8	−16	0	Right thalamus

Table 3
Regions of significant negative correlations between cerebral blood flow and T2-hyperintense lesion volume in MS patients using age, gender and duration of illness as nuisance variables.

Cluster size	*Z* score	*x*	*y*	*z*	Brain region
16	3.62	40	56	0	Right frontal lobe
35	3.98	−64	−44	32	Left parietal lobe
49	4.33	60	−40	40	Right parietal lobe
11	4.17	−60	−20	−16	Left temporal lobe
9	3.61	64	−4	−16	Right temporal lobe
68	4.29	−36	16	−8	Left insula
24	3.59	56	8	0	Right insula
23	4.59	−12	16	0	Left caudate
11	3.55	−12	−8	8	Left thalamus
9	3.42	8	−16	8	Right thalamus
12	3.37	4	−48	32	Right posterior cingulate
	3.33	−4	−44	40	Left posterior cingulate

Acknowledgments

We are grateful to Ms. Yuriko Suzuki at Philips for helpful discussions. This study was supported by Health and Labour Sciences Research Grants (Comprehensive Research on Disability, Health, and Welfare, #H23-seisin-young scientist 013; #H21-kokoro-002), an Intramural Research Grant for Neurological and Psychiatric Disorders of NCNP and "Understanding of molecular and environmental bases for brain health" carried out under the Strategic Research Program for Brain Sciences of the Ministry of Education, Culture, Sports, Science and Technology of Japan.

References

[1] Brownell B, Hughes JT. The distribution of plaques in the cerebrum in multiple sclerosis. J Neurol Neurosurg Psychiatry 1962;25:315-20.
[2] Dawson JW. The histology of multiple sclerosis. Trans R Soc (Edinb) 1916;50:517-740.
[3] Dinkler M. Zur Kasuistik der multiplen Herdsklerose des Gehirns und Ruckenmarks. Deuts Zeits f Nervenheilk 1904;26:233-47.
[4] Sander M. Hirnrindenbefunde bei multipler Sklerose. Monatschrift Psychiatrie Neurol 1898;IV:427-36.
[5] Schob F. Ein Beitrag zur pathologischen Anatomie der multiplen Sklerose. Monatschrift Psychiatrie Neurol 1907;22:62-87.
[6] Geurts JJ, Barkhof F. Grey matter pathology in multiple sclerosis. Lancet Neurol 2008;7:841-51.
[7] Blinkenberg M, Rune K, Jensen CV, Ravnborg M, Kyllingsbaek S, Holm S, et al. Cortical cerebral metabolism correlates with MRI lesion load and cognitive dysfunction in MS. Neurology 2000;54:558-64.
[8] Derache N, Marié RM, Constans JM, Defer GL. Reduced thalamic and cerebellar rest metabolism in relapsing-remitting multiple sclerosis, a positron emission tomography study: correlations to lesion load. J Neurol Sci 2006;245:103-9.
[9] Inglese M, Park SJ, Johnson G, Babb JS, Miles L, Jaggi H, et al. Deep gray matter perfusion in multiple sclerosis: dynamic susceptibility contrast perfusion magnetic resonance imaging at 3 T. Arch Neurol 2007;64:196-202.
[10] Law M, Saindane AM, Ge Y, Babb JS, Johnson G, Mannon LJ, et al. Microvascular abnormality in relapsing-remitting multiple sclerosis: perfusion MR imaging findings in normal-appearing white matter. Radiology 2004;231:645-52.
[11] Lycke J, Wikkelsö C, Bergh AC, Jacobsson L, Andersen O. Regional cerebral blood flow in multiple sclerosis measured by single photon emission tomography with technetium-99 m hexamethylpropyleneamine oxime. Eur Neurol 1993;33:163-7.

[12] Papadaki EZ, Mastorodemos VC, Amanakis EZ, Tsekouras KC, Papadakis AE, Tsavalas ND, et al. White matter and deep gray matter hemodynamic changes in multiple sclerosis patients with clinically isolated syndrome. Magn Reson Med 2012;68:1932-42.
[13] Paulesu E, Perani D, Fazio F, Comi G, Pozzilli C, Martinelli V, et al. Functional basis of memory impairment in multiple sclerosis: a [18 F]FDG PET study. Neuroimage 1996;4:87-96.
[14] Rashid W, Parkes LM, Ingle GT, Chard DT, Toosy AT, Altmann DR, et al. Abnormalities of cerebral perfusion in multiple sclerosis. J Neurol Neurosurg Psychiatry 2004;75:1288-93.
[15] Saindane AM, Law M, Ge Y, Johnson G, Babb JS, Grossman RI. Correlation of diffusion tensor and dynamic perfusion MR imaging metrics in normal-appearing corpus callosum: support for primary hypoperfusion in multiple sclerosis. AJNR Am J Neuroradiol 2007;28:767-72.
[16] Varga AW, Johnson G, Babb JS, Herbert J, Grossman RI, Inglese M. White matter hemodynamic abnormalities precede sub-cortical gray matter changes in multiple sclerosis. J Neurol Sci 2009;282:28-33.
[17] Aslan S, Xu F, Wang PL, Uh J, Yezhuvath US, van Osch M, et al. Estimation of labeling efficiency in pseudocontinuous arterial spin labeling. Magn Reson Med 2010;63:765-71.
[18] Wolff SD, Balaban RS. Magnetization transfer contrast (MTC) and tissue water proton relaxation in vivo. Magn Reson Med 1989;10:135-44.
[19] Detre JA, Alsop DC. Perfusion magnetic resonance imaging with continuous arterial spin labeling: methods and clinical applications in the central nervous system. Eur J Radiol 1999;30:115-24.
[20] Dai W, Garcia D, de Bazelaire C, Alsop DC. Continuous flow-driven inversion for arterial spin labeling using pulsed radio frequency and gradient fields. Magn Reson Med 2008;60:1488-97.
[21] Wong EC. Vessel-encoded arterial spin-labeling using pseudocontinuous tagging. Magn Reson Med 2007;58:1086-91.
[22] Wu WC, Fernandez-Seara M, Detre JA, Wehrli FW, Wang J. A theoretical and experimental investigation of the tagging efficiency of pseudocontinuous arterial spin labeling. Magn Reson Med 2007;58:1020-7.
[23] Polman CH, Reingold SC, Banwell B, Clanet M, Cohen JA, Filippi M, et al. Diagnostic criteria for multiple sclerosis: 2010 revisions to the McDonald criteria. Ann Neurol 2011;69:292-302.
[24] Kurtzke JF. Rating neurologic impairment in multiple sclerosis: an expanded disability status scale (EDSS). Neurology 1983;33:1444-52.
[25] Wang Z, Aguirre GK, Rao H, Wang J, Fernández-Seara MA, Childress AR, et al. Empirical optimization of ASL data analysis using an ASL data processing toolbox: ASLtbx. Magn Reson Imaging 2008;26:261-9.
[26] Cavuşoğlu M, Pfeuffer J, Uğurbil K, Uludağ K. Comparison of pulsed arterial spin labeling encoding schemes and absolute perfusion quantification. Magn Reson Imaging 2009;27:1039-45.
[27] Lu H, Clingman C, Golay X, van Zijl PC. Determining the longitudinal relaxation time (T1) of blood at 3.0 tesla. Magn Reson Med 2004;52:679-82.
[28] Wang J, Zhang Y, Wolf RL, Roc AC, Alsop DC, Detre JA. Amplitude-modulated continuous arterial spin-labeling 3.0-T perfusion MR imaging with a single coil: feasibility study. Radiology 2005;235:218-28.
[29] Pernet C, Andersson J, Paulesu E, Demonet JF. When all hypotheses are right: a multifocal account of dyslexia. Hum Brain Mapp 2009;30:2278-92.
[30] Carter CS, Heckers S, Nichols T, Pine DS, Strother S. Optimizing the design and analysis of clinical functional magnetic resonance imaging research studies. Biol Psychiatry 2008;64:842-9.
[31] Amann M, Achtnichts L, Hirsch JG, Naegelin Y, Gregori J, Weier K, et al. 3D GRASE arterial spin labelling reveals an inverse correlation of cortical perfusion with the white matter lesion volume in MS. Mult Scler 2012;18:1570-6.
[32] Fischer JS, Rudick RA, Cutter GR, Reingold SC. The Multiple Sclerosis Functional Composite Measure (MSFC): an integrated approach to MS clinical outcome assessment. National MS Society Clinical Outcomes Assessment Task Force. Mult Scler 1999;5:244-50.
[33] Riccitelli G, Rocca MA, Pagani E, Martinelli V, Radaelli M, Falini A, et al. Mapping regional grey and white matter atrophy in relapsing-remitting multiple sclerosis. Mult Scler 2012;18:1027-37.
[34] Cifelli A, Arridge M, Jezzard P, Esiri MM, Palace J, Matthews PM. Thalamic neurodegeneration in multiple sclerosis. Ann Neurol 2002;52:650-3.
[35] Behrens TE, Johansen-Berg H, Woolrich MW, Smith SM, Wheeler-Kingshott CA, Boulby PA, et al. Noninvasive mapping of connections between human thalamus and cortex using diffusion imaging. Nat Neurosci 2003;6:750-7.
[36] Buffon F, Molko N, Hervé D, Porcher R, Denghien I, Pappata S, et al. Longitudinal diffusion changes in cerebral hemispheres after MCA infarcts. J Cereb Blood Flow Metab 2005;25:641-50.

BRAIN RESEARCH 1499 (2013) 61–68

Available online at www.sciencedirect.com

SciVerse ScienceDirect

www.elsevier.com/locate/brainres

Brain Research

Research Report

Multimodal image analysis of sensorimotor gating in healthy women

Miho Ota[a,*], *Noriko Sato*[b], *Junko Matsuo*[a], *Yukiko Kinoshita*[a], *Yumiko Kawamoto*[a], *Hiroaki Hori*[a], *Toshiya Teraishi*[a], *Daimei Sasayama*[a], *Kotaro Hattori*[a], *Satoko Obu*[a], *Yasuhiro Nakata*[b], *Hiroshi Kunugi*[a]

[a]*Department of Mental Disorder Research, National Institute of Neuroscience, National Center of Neurology and Psychiatry, 4-1-1 Ogawa-Higashi, Kodaira, Tokyo 187–8502, Japan*

[b]*Department of Radiology, National Center of Neurology and Psychiatry, 4-1-1 Ogawa-Higashi, Kodaira, Tokyo 187-8551, Japan*

ARTICLE INFO

Article history:
Accepted 29 December 2012
Available online 16 January 2013

Keywords:
Diffeomorphic anatomical registration using exponentiated lie algebra
Diffusion tensor imaging
Prepulse inhibition
Tract-based spatial statistics

ABSTRACT

Prepulse inhibition (PPI) deficits have been reported in individuals with schizophrenia and other psychiatric disorders with dysfunction of the cortico–striato–pallido–thalamic circuit. The purpose of this study was to investigate the structural neural correlates of PPI by using magnetic resonance imaging (MRI) metrics. The subjects were 53 healthy women (mean age; 40.7±11.3 years). We examined the possible relationships between PPI and diffusion tensor imaging (DTI) metrics to estimate white matter integrity and gray matter volume analyzed using the DARTEL (diffeomorphic anatomical registration through exponentiated lie) algebra method. There were significant correlations between DTI metrics and PPI in the parahippocampal region, the anterior limb of the internal capsule, the ventral tegmental area, the thalamus and anterior thalamic radiations, the left prefrontal region, the callosal commissural fiber, and various white matter regions. There were also positive correlations between PPI and gray matter volume in the bilateral parietal gyri and the left inferior prefrontal gyrus at a trend level. The present study revealed evidence of a relationship between PPI and the integrity of white matter. This result was compatible with the previous suggestion that PPI would be modulated by the cortico-striato-thalamic-pallido-pontine circuit.

Abbreviations: 3-dimensional (3D), blood oxygenation level-dependent (BOLD); cerebrospinal fluid (CSF), diffeomorphic anatomical registration using exponentiated lie algebra (DARTEL); diffusion tensor imaging (DTI), echo time (TE); false discovery rate (FDR), family-wise error (FWE); field of view (FOV), fluid attenuation inversion recovery (FLAIR); fractional anisotropy (FA), functional magnetic resonance imaging (fMRI); mean diffusivity (MD), Mini-International Neuropsychiatric Interview (MINI); positron emission tomography (PET), prepulse inhibition (PPI); repetition time (TR), statistical parametric mapping (SPM); threshold-free cluster enhancement (TFCE), tract-based spatial statistics (TBSS). voxel-based morphometry (VBM).

*Corresponding author. Fax: +81 42 346 2094.
E-mail address: ota@ncnp.go.jp (M. Ota).

0006-8993/$ - see front matter © 2013 Elsevier B.V. All rights reserved.
http://dx.doi.org/10.1016/j.brainres.2012.12.044

1. Introduction

The startle reflex can be attenuated when the startling stimulus is preceded by a weak non-startling prepulse, in a process called prepulse inhibition (PPI). The degree to which such a prepulse inhibits the startle reflex in PPI is used as a measure of sensorimotor gating. Disruptions in information processing and attention have long been thought of as one of the hallmarks of schizophrenia (McGhie and Chapman, 1961), and PPI has been suggested as a neurophysiologic measure of information processing abnormalities in schizophrenia (Cadenhead and Braff, 1999).

There is evidence from animal studies that PPI is modulated by forebrain circuits involving the prefrontal cortex, thalamus, hippocampus, amygdala, nucleus accumbens, striatum, and globus pallidus (Koch and Schnitzler, 1997; Swerdlow and Geyer, 1998; Swerdlow et al., 2001). Deficient PPI is observed in several neuropsychiatric disorders characterised by abnormalities in the cortico-striato-thalamic-pontine circuitry (Braff et al., 2001; Swerdlow et al., 2008). Previous neuroimaging studies using structural brain images revealed the neural correlates of PPI in the prefrontal and orbitofrontal cortex, hippocampus extending to the parahippocampal gyrus, the basal ganglia including parts of putamen, the globus pallidus, and the nucleus accumbens, posterior cingulate, superior temporal gyrus, and thalamus (Kumari et al., 2005, 2008a). Several functional magnetic resonance imaging (fMRI) studies showed that PPI is associated with increased bilateral activation in the striatum extending to the hippocampus, insula, thalamus, and inferior frontal, middle temporal, and inferior parietal lobes (Hazlett et al., 2001, 2008; Kumari et al., 2003, 2008a). A regression analysis demonstrated a linear relationship between PPI and blood oxygenation level-dependent (BOLD) activity in the thalamus, nucleus accumbens, and inferior parietal region (Kumari et al., 2003). Positron emission tomography (PET) study also detected an association between PPI and the prefrontal and inferior parietal cortices' glucose metabolism (Hazlett et al., 1998). Although it is known that PPI disruption resulted from the interruption of the cortico–striato–thalamic–pontine neural circuit, to our knowledge there has been no study verifying the integrity of white matter using diffusion tensor imaging (DTI).

The present study was conducted to investigate the structural basis of PPI deficits using DTI and volumetry analysis. We hypothesized that PPI would be correlated with components in the hippocampus/temporal lobe, basal ganglia, cingulate gyrus, and frontal and parietal regions.

2. Results

Initially, we examined the correlation between the gray matter volume and % PPI using DARTEL (diffeomorphic anatomical registration using exponentiated lie). There was no significant correlation between them; however, there were nominal trends between % PPI with 90 dB prepulse and gray matter volume in the bilateral parietal gyri and left inferior prefrontal regions ($p<0.005$ uncorrected) (Fig. 1(A)), and between % PPI with 86 dB prepulse and gray matter volume in the left parietal and medial frontal regions ($p<0.005$ uncorrected) (Fig. 1(B)).

We then examined correlation between % PPI and DTI. Significant positive correlations were observed between fractional anisotropy (FA) value and % PPI with 90 dB prepulse in the right ventral tegmental area, left anterior limbs of the internal capsule, bilateral thalami, and the left inferior prefrontal region, bilateral medial frontal regions, and bilateral parietal regions ($p<0.001$ uncorrected) (Fig. 2(A) to (F)), however, we could detect correlation between % PPI with 86 dB prepulse and FA values only in the inferior prefrontal region (Fig. 2(G)) ($p<0.001$ uncorrected). In addition, analysis using the skeletonized FA data showed that there were significant positive correlations between FA value and % PPI with 90 dB prepulse in the parahippocampal region, orbitofrontal region, bilateral temporal–inferior parietal regions, internal capsule,

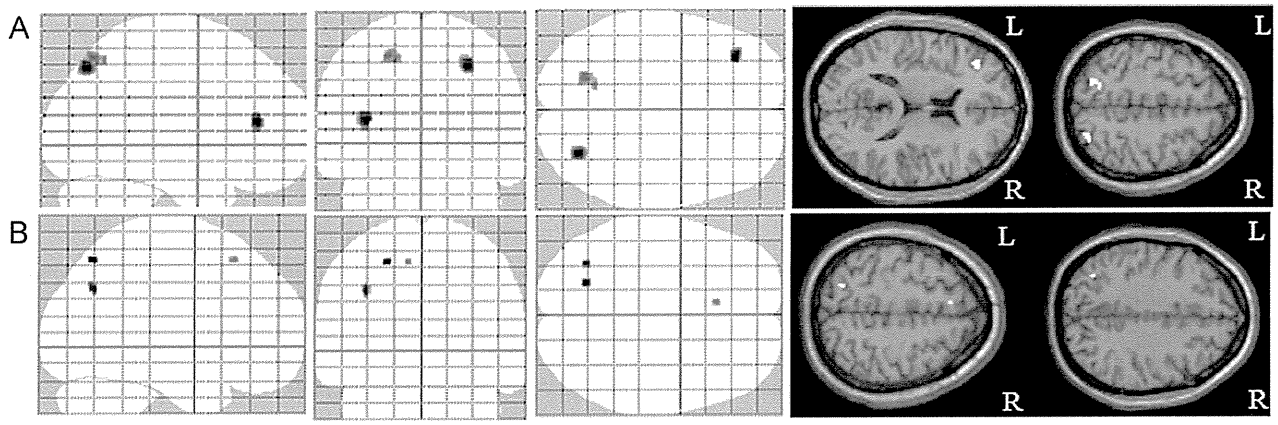

Fig. 1 – Brain areas in which % PPI and gray matter volume showed correlation. There was no significant correlation between % PPI and gray matter volume. However, a nominal trend was found in the bilateral parietal regions and left inferior prefrontal regions (A) ($p<0.005$ uncorrected). Likewise, there was a nominal correlation between % PPI with 86 dB prepulse and gray matter volume in the left parietal and medial frontal regions (B) ($p<0.005$ uncorrected). Age and whole brain volume were controlled. L, left; R, right.

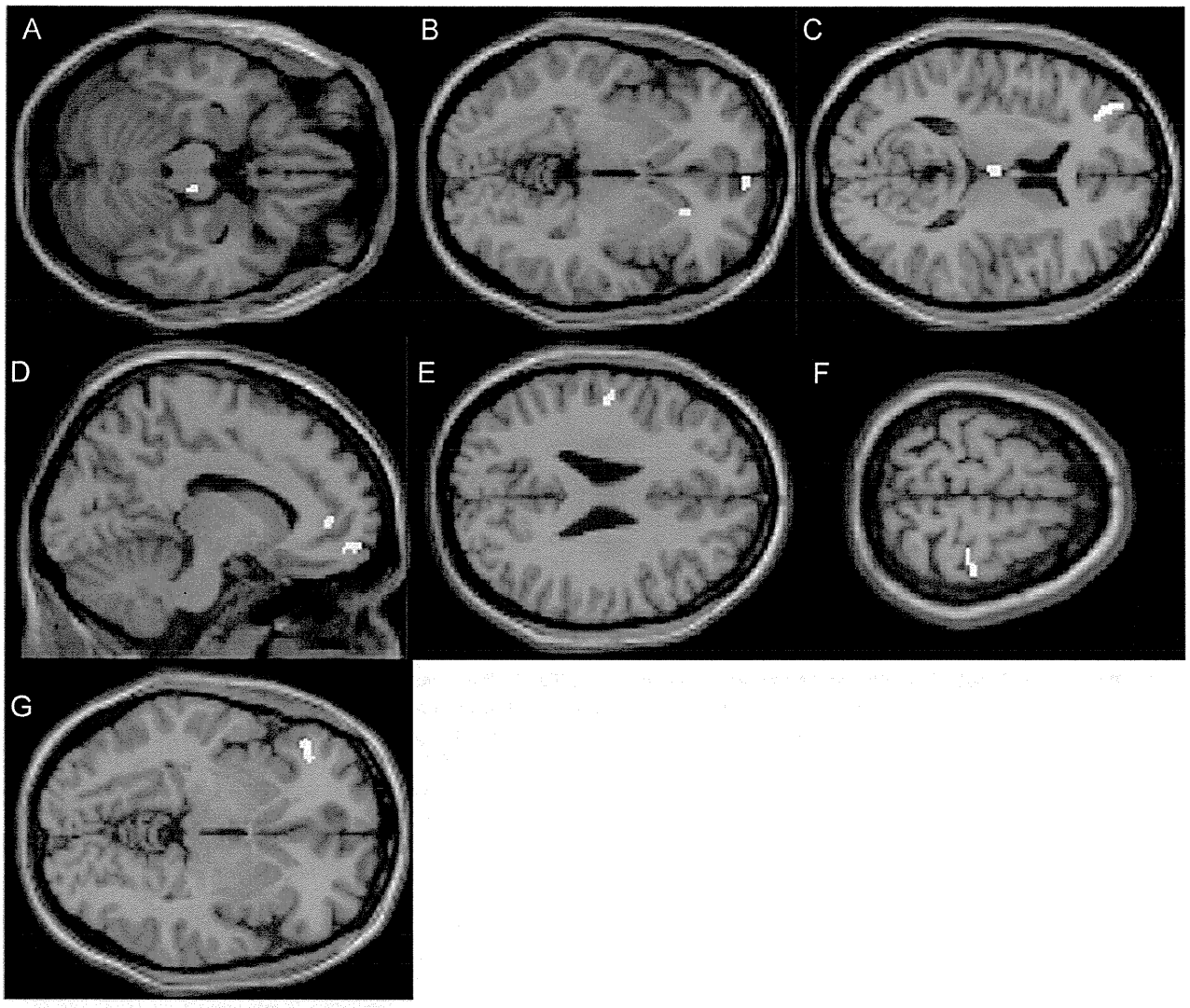

Fig. 2 – Brain areas in which % PPI and FA values correlated. There were positive correlations between % PPI with 90 dB of prepulse and FA values in the right ventral tegmental area (A), left anterior limbs of internal capsule (B), bilateral thalami, and left inferior prefrontal region (C), bilateral medial frontal regions ((B), (D)), and bilateral parietal regions ((E) and (F)) ($p<0.001$ uncorrected). Correlation between % PPI with 86 dB of prepulse and FA values was seen only in the inferior prefrontal region (G) ($p<0.001$ uncorrected). Age was controlled. L, left; R, right.

thalamus, anterior thalamic radiations, posterior cingulate, and callosal commissural fibers ($p<0.05$, family-wise error (FWE) rate is controlled) (Fig. 3(A) to (D)). On the other hand, there were no significant correlation between % PPI with 86 dB prepulse and FA value, and only nominal trends were revealed in similar regions (Fig. 3(E) to (H)) ($p<0.1$; FWE rate is controlled).

There were significantly positive correlations between % PPI and the mean diffusivity (MD) values in many regions throughout the brain (90 dB; Fig. 4(A), 86 dB; Fig. 4(B)). To be more conservative, we corrected for multiple testing by false discovery rate (FDR) and set the critical p-value as <0.01(90 dB), and by FWE and set the critical p-value as <0.05 (86 dB). After this procedure, the correlations of PPI with MD values in the left inferior prefrontal region remained significant (Fig. 4(A) and (B), the right column).

3. Discussion

To our knowledge, this is the first study that used DTI to examine the possible relationships between PPI and brain structure in healthy subjects. Significant correlations were noted between PPI and DTI metrics in the ventral tegmental area, parahippocampus, callosal commissural fiber, thalamus, anterior thalamic radiation, internal capsule, posterior cingulate, and temporal and parietal regions. There were nominal trends between PPI and gray matter volume in the left inferior prefrontal region and bilateral parietal regions. Our results are consistent with previous neuroimaging studies using structural MRI and fMRI and pharmacological studies (Hazlett et al., 2001; Kumari et al., 2005; Swerdlow et al., 2001).

Consistent with the consensus regarding PPI in the rat, a number of psychiatric and neurological disorders characterized

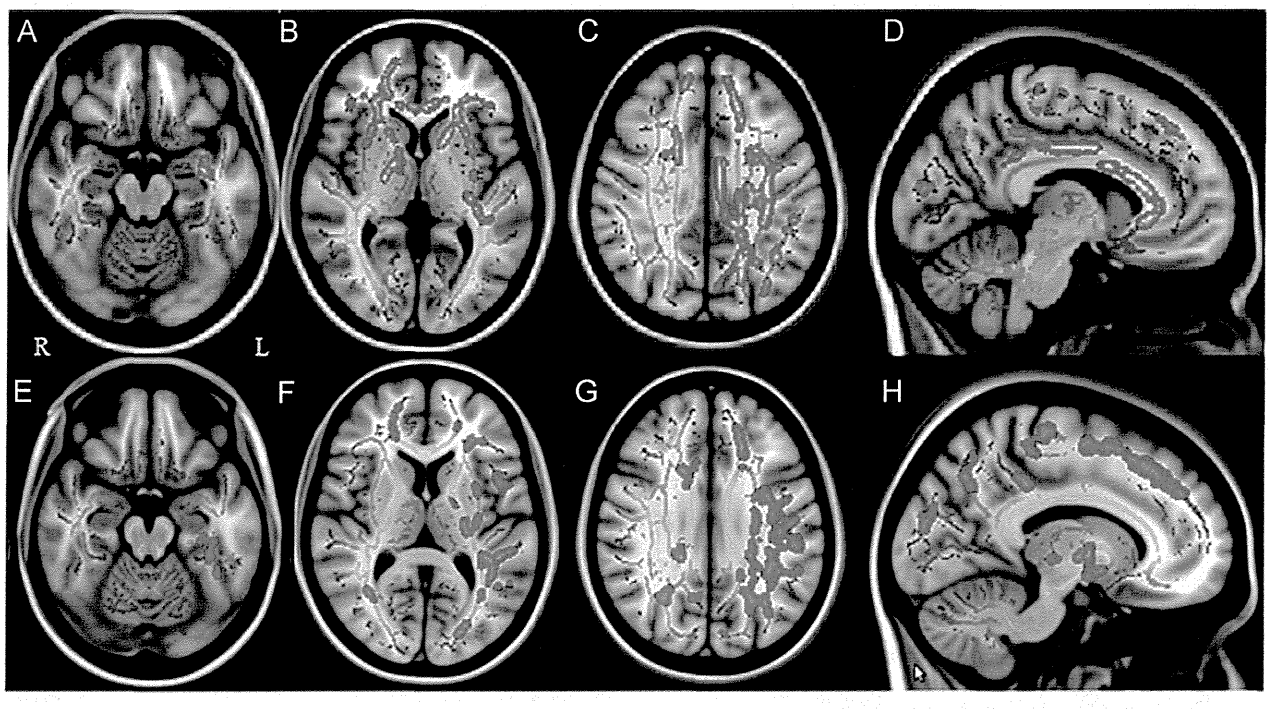

Fig. 3 – Brain areas in which % PPI and FA values correlated using TBSS. There were positive correlations between % PPI with 90 dB of prepulse and FA values in the parahippocampal region (A), orbitofrontal region (A), temporal–parietal regions ((B) and (C)), internal capsules (B), thalamus and anterior thalamic radiations ((B) and (C)), posterior cingulate ((C) and (D)), and anterior dominant callosal commissural fibers ((B) and (D)) revealed by tract-based spatial statistics (TBSS) ($p<0.05$; family-wise error rate is controlled). On the other hand, there were no significant correlations between % PPI with 86 dB of prepulse and FA values, however, a nominal trend was detected in similar regions ((E) to (H)) ($p<0.1$; family-wise error rate is controlled). Age was controlled. The skeleton, shown in green, is thresholded at 0.2 and overlaid onto the MNI152 space. L, left; R, right. (For interpretation of the references to colour in this figure legend, the reader is referred to the web version of this article.)

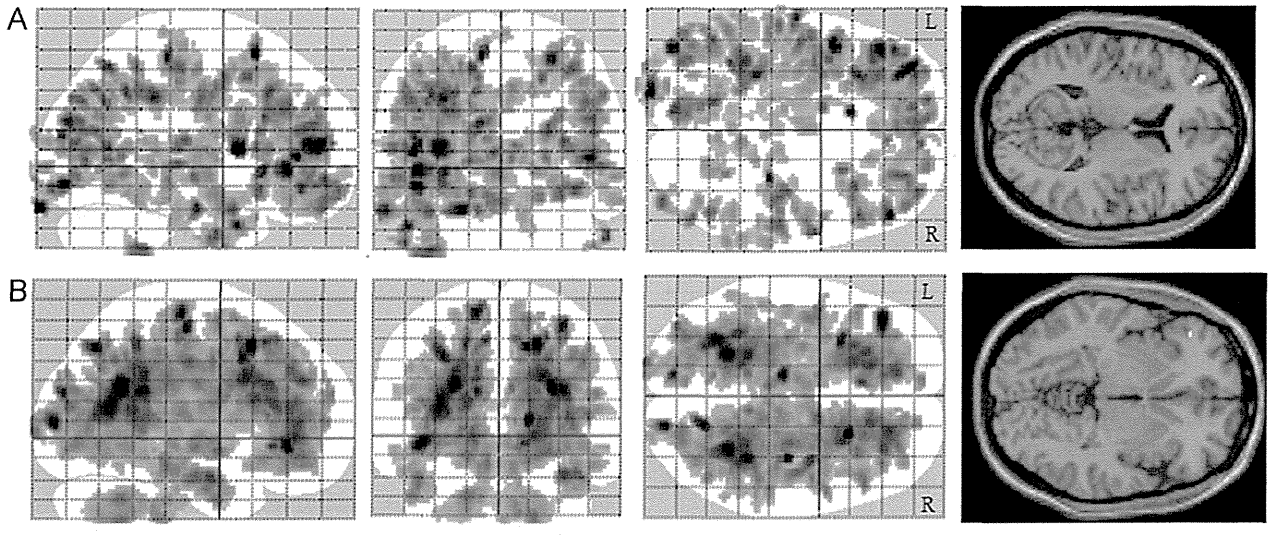

Fig. 4 – Brain areas in which % PPI and MD values correlated. There were negative correlations between % PPI with 90 (A) and 86 dB (B) of prepulse and MD values in several areas throughout the brain ($p<0.001$ uncorrected). The right column showed that the correlations remained when we re-analyzed the correlation between PPI and MD values in the left inferior prefrontal region (90 dB; $p<0.01$ [false discovery rate], 86 dB; $p<0.05$ [family-wise error rate]). L, left; R, right.

by abnormalities at some level in the cortico–striato–thalamic–pontine circuitry (Braff et al., 2001; Swerdlow et al., 2008) and in the cortico–striato–pallido–thalamic brain substrate (Perry et al., 2004; Swerdlow et al., 2008) showed the PPI deficient. Previous neuroimaging studies revealed the correlation between PPI and regional brain using structural brain images (Kumari et al., 2005,

2008b), and fMRI (Hazlett et al., 2001, 2008; Kumari et al., 2003, 2007, 2008a). Here we found significant correlations between PPI and DTI metrics in the parahippocampus, the internal capsule, the circumference of anterior thalamic radiation and the parietal region. In light of these observations, PPI may be regulated through an amygdala – basal ganglia – prefrontal and parietal circuit. There is evidence from animal studies that PPI is mediated by brain stem circuits involving the inferior colliculus, superior colliculus, pedunculopontine tegmental nucleus, laterodorsal tegmental nucleus, substantia nigra pars reticulata, and caudal pontine reticular nucleus (Fendt et al., 2001). In the present study, we detected a correlation between FA in the ventral tegmental area and % PPI, a finding that is compatible with this previous evidence.

As described above, previous studies showed that PPI is influenced by many regions throughout the brain, and PPI is thought to be affected by the transmission of information. We therefore hypothesized that to evaluate the relation between PPI and the brain, the use of DTI – which shows the condition of the neural fibers – would be effective. Our DTI results suggested that a large area of the brain is involved in deficits in PPI, compared to the foregoing studies focusing on the gray matter. This may be due to the ability of DTI to delineate neural pathways. Furthermore, we detected more correlations between % PPI and brain metrics when prepulse was 90 dB than when it was 86 dB. Previous studies showed that % PPI at the prepulse intensity of 90 dB was higher compared with that at 86 dB, and that the difference in % PPI between patients with schizophrenia and healthy controls became most significant when prepulse was 90 dB (Kunugi et al., 2007; Takahashi et al., 2008; Moriwaki et al., 2009). These points may suggest that % PPI with 90 dB of prepulse is the best condition to reflect his/her own information processing and attention.

Regarding the volumetric analysis, we could not detect any significant relationship between the PPI and gray matter volume, although the data showed a nominal trend of a relationship in the inferior frontal gyrus and bilateral parietal regions. As to the association between the inferior prefrontal region and PPI, we detected this relationship by all metrics used in this study. This connection was previously detected in an MRI volumetric study (Kumari et al., 2005). However, 10 men and 14 women took part in that study. Previous studies showed a gender difference in PPI (Kumari. et al., 2004), but we evaluated only female subjects. We failed to detect any significant correlation between PPI and gray matter volume. The inconsistent results between previous studies and ours may be attributable, at least in part, to the fact that we examined only females who showed a narrow range of PPI. In conjunction with this, our study included only healthy women whose % PPI was changeable along with the menstrual cycle status (Swerdlow et al., 1997). Further studies work with information on menstrual cycle and studies on male subjects are necessary to address this issue.

In conclusion, the present study examined structural neural correlates of PPI and revealed evidence of a relationship between PPI and the integrity of white matter in healthy women. These observations confirm the involvement of these regions in human PPI as suggested by previous relevant data. Further research should extend the present methods in studies of clinical populations.

4. Experimental procedures

4.1. Sample

The subjects were 63 healthy females who were recruited from the community through local magazine advertisements and our website announcement. The participants were interviewed for enrollment using the Japanese version of the Mini-International Neuropsychiatric Interview (MINI) (Otsubo et al., 2005; Sheehan et al., 1998) by research psychiatrists, and only those who demonstrated no history of psychiatric illness or contact with psychiatric services were enrolled in the study. Participants were excluded if they had a prior medical history of central nervous system disease or severe head injury. In addition, 10 non-responders to the startle stimulus (see the "*Prepulse inhibition measure*" below) were also excluded from the analysis. As a consequence, 53 healthy females (mean age; 40.7 ± 11.3 years, education; 14.8 ± 2.7 years) took part in the study.

Written informed consent was obtained for participation in the study from all subjects, and the study was approved by the Ethics Committee of the National Center of Neurology and Psychiatry, Tokyo, Japan.

4.2. Prepulse inhibition measure

Our equipment, setup, and standard PPI testing procedures have been described in detail (Kunugi et al., 2007). The startle reflex to acoustic stimuli was measured using the Startle Reflex Test Unit for Humans (O'Hara Medical, Tokyo). Subjects refrained from smoking for at least 20 min prior to the test. Broadband white noise (50 to 24,000 Hz) at 70 dB was presented as the background noise and was continuous throughout the session. Acoustic startle stimuli of the broadband white noise were presented through headphones.

During the initial 3 min of each session, the background noise alone was given for acclimation. In total, 35 startle-response trials were recorded in a session. These trials consisted of three blocks. In the first block, the subject's startle response to a pulse (sound pressure: 115 dB; duration: 40 ms) alone was recorded five times. In the second block, the subject's startle response to the same pulse with or without a prepulse (sound pressure: 86 or 90 dB; duration: 20 ms; lead interval [onset to onset]: 60 or 120 ms) was measured five times for each condition. The differential conditions of trials were presented in a pseudo-random order; however, the order was the same for all of the subjects. In the third and final block, the startle response to the pulse alone was again measured five times. The intertrial intervals (15 s on average, range 10 to 20 s) were randomly changed. The entire session lasted approximately 15 min. The mean % PPI of startle magnitude was calculated using the following formula, because in a previous study this condition showed the best sensitivity to differentiate between schizophrenic patients and healthy subjects (Kunugi et al., 2007):

% PPI = 100 × (magnitude on pulse-alone trials − magnitude on prepulse trials {sound pressure: 86 dB and 90 dB; lead

interval: 120 ms, right eye})/magnitude on pulse-alone trials in the 2nd block.

The mean % PPI of the 53 subjects were 45.9±54.7 under the terms of 86 dB, and 58.8±39.8 of 90 dB. We defined *a priori* the "non-responders" to the startle stimuli as those subjects for whom the average value of the startle magnitude in the pulse-alone trials was <0.05 (digital unit), and the non-responders were excluded from the analysis.

4.3. MRI data acquisition

4.3.1. Data acquisition

MR imaging was performed on a Magnetom Symphony 1.5-T system (Siemens, Erlangen, Germany). High spatial resolution, 3-dimensional (3D) T1-weighted images of the brain were obtained for the morphometric study. The 3D T1-weighted images were scanned in the sagittal plane (echo time (TE)/repetition time (TR): 2.64/1580 ms; flip angle: 15°; effective slice thickness: 1.23 mm; slab thickness: 177 mm; matrix: 208 × 256; field of view (FOV): 256 × 315 mm^2; acquisition: (1), yielding 144 contiguous slices through the head.

DTI was performed in the axial plane (TE/TR: 106/11,200 ms; FOV: 240 × 240 mm^2; matrix: 96 × 96; 75 continuous transverse slices; slice thickness 2.5 mm with no interslice gap; acquisitions: (2). Diffusion was measured along 12 non-collinear directions with the use of a diffusion-weighted factor, *b*, in each direction for 1000 s/mm^2, and one image was acquired without use of a diffusion gradient. The DTI examination took approx. 6 min. In addition to DTI and 3D T1-weighted images, conventional axial T2-weighted images (TE/TR: 95/3500 ms; flip angle: 150°; slice thickness: 5 mm; intersection gap: 1.75 mm; matrix: 448 × 512; FOV: 210 × 240 mm^2; acquisitions: (1), and fluid attenuation inversion recovery (FLAIR) images in the axial plane (TE/TR: 101/8800 ms; flip angle: 150°; slice thickness: 3 mm; intersection gap: 1.75 mm; matrix: 448 × 512; FOV: 210 × 240 mm^2; acquisition: (1) were acquired to exclude cerebrovascular disease. On conventional MRI, no abnormal findings were detected in the brain in any subject.

4.3.2. Diffeomorphic anatomical registration using exponentiated lie analysis

The raw 3D T1-weighted volume data were transferred to a workstation. A preprocessing step of voxel-based morphometry (VBM) in Statistical Parametric Mapping (SPM) was improved with the DARTEL registration method (Ashburner, 2007). This technique, being more deformable, notably improves the realignment of small inner structures (Yassa and Stark, 2009). Calculations and image matrix manipulations were performed using SPM8 running on MATLAB R2007a software (MathWorks, Natick, MA). MR imaging data were analyzed using DARTEL as a toolbox for SPM8 to create a set of group-specific templates. The brain images were segmented, normalized, and modulated by using these templates. The output images were still in the average brain space. Additional warping from the Montreal Neurologic Institute space was given to the brain images. Then, gray matter probability values were smoothed by using an 8-mm full-width at half-maximum Gaussian kernel.

4.3.3. DTI procedure

The DTI data sets were analyzed using DtiStudio (Jiang et al., 2006). The diffusion tensor parameters were calculated on a pixel-by-pixel basis, and FA and MD map and $b=0$ image were calculated according to Wakana et al. (2004).

4.3.4. SPM analysis

To estimate the relationships between brain morphology and % PPI, FA and MD images were analyzed using an optimized VBM technique. The data were analyzed using SPM5 software running on MATLAB 7.0. The images were processed using an optimized VBM script. The details of this process are described elsewhere (Good et al., 2001). First, each individual 3D-T1 image was coregistered and resliced to its own $b=0$ image. Next, the coregistered 3D-T1 image was normalized to the "avg152T1" image regarded as the anatomically standard image in SPM5. Finally, the transformation matrix was applied to FA and MD maps. Further, to avoid the effect of diffusivity of cerebrospinal fluid (CSF), MD images were masked with the CSF image derived from the segmented individual 3D-T1 image. Each map was then spatially smoothed with a 6-mm full-width at half-maximum Gaussian kernel in order to decrease spatial noise and compensate for the inexactitude of normalization following the "rule of thumb" developed for fMRI and PET studies (Snook et al., 2007).

4.3.5. Tract-based spatial statistics (TBSS) analysis

The processing technique known as "tract-based spatial statistics (TBSS) analysis" projects DTI data onto a common pseudo-anatomical skeleton instead of trying to match each and every voxel in different subjects, and therefore does not need smoothing (Smith et al., 2006). TBSS is available as part of the FSL 4.1 software package (Smith et al., 2004). The TBSS script runs a nonlinear registration, aligning all FA images to the FMRIB58_FA template, which is supplied with FSL. The script then takes the target and affine-aligns it into a 1 × 1 × 1 mm MNI152 space. Once this is done, each subject's FA image has the nonlinear transform to the target and then the affine transform to MNI152 space is applied, resulting in a transformation of the original FA image into MNI152 space. Next, TBSS creates the mean of all aligned FA images and applies thinning of the local tract structure to create a skeletonized mean FA image. In order to exclude areas of low FA and/or high intersubject variability from a statistical analysis, TBSS thresholds a mean FA skeleton with a certain FA value, typically 0.2. The resulting binary skeleton mask is a pseudo-anatomical representation of the main fiber tracks, and defines the set of voxels used in all subsequent processing. Finally, TBSS projects each subject's aligned FA image onto the skeleton. This results in skeletonized FA data. It is this file that is used for the voxelwise statistics.

4.3.6. Statistical analysis

Statistical analyses were performed using SPM5 software (Welcome Department of Imaging Neuroscience, London, UK). Correlations between regional gray matter volume and % PPI with 86 and 90 dB of prepulse were assessed using the subjects' age, length of education, and whole brain volume as nuisance variables, and FA and MD value maps and % PPI

were assessed using age and education year as nuisance variables. Only correlations that met these criteria were deemed significant. In this case, a seed level of $p<0.001$ (uncorrected) and a cluster level of $p<0.05$ (uncorrected) were selected.

Skeletonized FA data were analyzed for revealing correlations with % PPI, controlling for age, using the FSL "Threshold-Free Cluster Enhancement (TFCE)" option in "randomise" with 5000 permutations, the script of which uses a permutation-based statistical inference that does not rely on a Gaussian distribution of voxels, and is run without having to define an initial cluster-forming threshold or carry out a large amount of data smoothing (Nichols and Holmes, 2002; Smith and Nichols, 2009). The significance level was set at the p-value of less than 0.05 with FWE rate correction for multiple comparisons.

Acknowledgments

This study was supported by Health and Labor Sciences Research Grants (Comprehensive Research on Disability, Health, and Welfare), Intramural Research Grant (24-11) for Neurological and Psychiatric Disorders of NCNP (M.O. and H.K.), "Understanding of molecular and environmental bases for brain health" carried out under the Strategic Research Program for Brain Sciences by the Ministry of Education, Culture, Sports, Science and Technology of Japan, and a grant from Core Research of Evolutional Science & Technology (CREST), Japan Science and Technology Agency (JST) (H.K.)

REFERENCES

Ashburner, J., 2007. A fast diffeomorphic image registration algorithm. NeuroImage 38, 95–113.

Braff, D.L., Geyer, M.A., Swerdlow, N.R., 2001. Human studies of prepulse inhibition of startle: normal subjects, patient groups, and pharmacological studies. Psychopharmacology (Berl) 156, 234–258.

Cadenhead, K.S., Braff, D.L., 1999. Schizophrenia spectrum disorders. In: Dawson, M.E., Schell, A.M., Bohmelt, A.H. (Eds.), Startle Modification: Implications for Neuroscience. Cognitive Science, and Clinical Science. Cambridge University Press, Cambridge, pp. 231–244.

Fendt, M., Liang, L., Yeomans, J.S., 2001. Brain stem circuits mediating prepulse inhibition of the startle reflex. Psychopharmacology 156, 216–224.

Good, C.D., Johnsrude, I., Ashburner, J., Henson, R.N.A., Friston, K.J., Frackowiak, R.S.J., 2001. Cerebral asymmetry and the effect of sex and handedness on brain structure: a voxel-based morphometric analysis of 465 normal adult human brains. NeuroImage 14, 685–700.

Hazlett, E.A., Buchsbaum, M.S., Haznedar, M.M., Singer, M.B., Germans, M.K., Schnur, D.B., Jimenez, E.A., Buchsbaum, B.R., Troyer, B.T., 1998. Prefrontal cortex glucose metabolism and startle eyeblink modification abnormalities in unmedicated schizophrenia patients. Psychophysiology 35, 186–198.

Hazlett, E.A., Buchsbaum, M.S., Tang, C.Y., Fleischman, M.B., Wei, T.C., Byne, W., Haznedar, M.M., 2001. Thalamic activation during an attention-to-prepulse startle modification paradigm: a functional MRI study. Biol. Psychiatry 50, 281–291.

Hazlett, E.A., Buchsbaum, M.S., Zhang, J., Newmark, R.E., Glanton, C.F., Zelmanova, Y., Haznedar, M.M., Chu, K.W., Nenadic, I., Kemether, L.J., Tang, C.Y., New, A.S., Siever, L.J., 2008. Frontal–striatal–thalamic mediodorsal nucleus dysfunction in schizophrenia-spectrum patients during sensorimotor gating. NeuroImage 42, 1164–1177.

Jiang, H., van Zijil, P.C., Kim, J., Pearlson, G.D., Mori, S., 2006. DtiStudio: resource program for diffusion tensor computation and fiber bundle tracking. Comput. Methods Programs Biomed. 81, 106–116.

Koch, M, Schnitzler, H, 1997. The acoustic startle response in rats: circuits mediating evocation, inhibition and potentiation. Behav. Brain Res. 89, 35–49.

Kumari, V., Aasen, I., Sharma, T., 2004. Sex differences in prepulse inhibition deficits in chronic schizophrenia. Schizophr. Res. 69, 219–235.

Kumari, V., Antonova, E., Geyer, M.A., 2008a. Prepulse inhibition and "psychosis-proneness" in healthy individuals: an fMRI study. Eur. Psychiatry 23, 274–280.

Kumari, V., Antonova, E., Geyer, M.A., Ffytche, D., Williams, S.C., Sharma, T., 2007. A fMRI investigation of startle gating deficits in schizophrenia patients treated with typical or atypical antipsychotics. Int. J. Neuropsychopharmacol. 10, 463–477.

Kumari, V., Antonova, E., Zachariah, E., Galea, A., Aasen, I., Ettinger, U., Mitterschiffthaler, M.T., Sharma, T., 2005. Structural brain correlates of prepulse inhibition of the acoustic startle response in healthy humans. NeuroImage 26, 1052–1058.

Kumari, V., Fannon, D., Geyer, M.A., Premkumar, P., Antonova, E., Simmons, A., Kuipers, E., 2008b. Cortical grey matter volume and sensorimotor gating in schizophrenia. Cortex 44, 1206–1214.

Kumari, V., Gray, J.A., Geyer, M.A., Ffytche, D., Mitterschiffthaler, M.T., Vythelingum, G.N., Williams, S.C.R., Simmons, A., Sharma, T., 2003. Neural correlates of prepulse inhibition in normal and schizophrenic subjects: a functional MRI Study. Psychiatry Res.: NeuroImage 122, 99–113.

Kunugi, H., Tanaka, M., Hori, H., Hashimoto, R., Saitoh, O., Hironaka, N., 2007. Prepulse inhibition of acoustic startle in Japanese patients with chronic schizophrenia. Neurosci. Res. 59, 23–28.

McGhie, A, Chapman, J., 1961. Disorders of attention and perception in early schizophrenia. Br. J. Med. Psychol. 34, 103–116.

Moriwaki, M., Kishi, T., Takahashi, H., Hashimoto, R., Kawashima, K., Okochi, T., Kitajima, T., Furukawa, O., Fujita, K., Takeda, M., Iwata, N., 2009. Prepulse inhibition of the startle response with chronic schizophrenia: a replication study. Neurosci. Res. 65, 259–262.

Nichols, T.E., Holmes, A.P., 2002. Nonparametric permutation tests for functional neuroimaging: a primer with examples. Hum. Brain. Mapp. 15, 1–25.

Otsubo, T., Tanaka, K., Koda, R., Shinoda, J., Sano, N., Tanaka, S., Aoyama, H., Mimura, M., Kamijima, K., 2005. Reliability and validity of Japanese version of the Mini-International Neuropsychiatric Interview. Psychiatry Clin. Neurosci. 59, 517–526.

Perry, W., Minassian, A., Feifel, D., 2004. Prepulse inhibition in patients with non-psychotic major depressive disorder. J. Affect. Disord. 81, 179–184.

Sheehan, D.V., Lecrubier, Y., Sheehan, K.H., Amorim, P., Janavs, J., Weiller, E., Hergueta, T., Baker, R., Dunbar, G.C., 1998. The Mini-International Neuropsychiatric Interview (M.I.N.I.): the development and validation of a structured diagnostic psychiatric interview for DSM-IV and ICD-10. J. Clin. Psychiatry 59, 22–57.

Smith, S.M., Jenkinson, M., Johansen-Berg, H., Rueckert, D., Nichols, T.E., Mackay, C.E., Watkins, K.E., Ciccarelli, O., Cader, M.Z., Matthews, P.M., Behrens, T.E., 2006. Tract-based

spatial statistics: voxelwise analysis of multi-subject diffusion data. NeuroImage 31, 1487–1505.

Smith, S.M., Jenkinson, M., Woolrich, M.W., Beckmann, C.F., Behrens, T.E., Johansen-Berg, H., Bannister, P.R., De Luca, M., Drobnjak, I., Flitney, D.E., Niazy, R.K., Saunders, J., Vickers, J., Zhang, Y., De Stefano, N., Brady, J.M., Matthews, P.M., 2004. Advances in functional and structural MR image analysis and implementation as FSL. NeuroImage 23 (1), S208–219.

Smith, S.M., Nichols, T.E., 2009. Threshold-free cluster enhancement: addressing problems of smoothing, threshold dependence and localisation in cluster inference. NeuroImage 44, 83–98.

Snook, L., Plewes, C., Beaulieu, C., 2007. Voxel based versus region of interest analysis in diffusion tensor imaging of neurodevelopment. NeuroImage 34, 243–252.

Swerdlow, N.R., Geyer, M.A., 1998. Using an animal model of deficient sensorimotor gating to study the pathophysiology and new treatments of schizophrenia. Schizophrenia Bull. 24, 285–301.

Swerdlow, N.R., Geyer, M.A., Braff, D.L., 2001. Neural circuit regulation of prepulse inhibition of startle in the rat: current knowledge and future challenges. Psychopharmacology 156, 194–215.

Swerdlow, N.R., Hartman, P.L., Auerbach, P.P., 1997. Changes in sensorimotor inhibition across the menstrual cycle: implications for neuropsychiatric disorders. Biol. Psychiatry 41, 452–460.

Swerdlow, N.R., Weber, M., Qu, Y., Light, G.A., Braff, D.L., 2008. Realistic expectations of prepulse inhibition in translational models for schizophrenia research. Psychopharmacology (Berl) 199, 331–388.

Takahashi, H., Iwase, M., Ishii, R., Ohi, K., Fukumoto, M., Azechi, M., Ikezawa, K., Kurimoto, R., Canuet, L., Nakahachi, T., Iike, N., Tagami, S., Morihara, T., Okochi, M., Tanaka, T., Kazui, H, Yoshida, T, Tanimukai, H, Yasuda, Y, Kudo, T, Hashimoto, R, Takeda, M., 2008. Impaired prepulse inhibition and habituation of acoustic startle response in Japanese patients with schizophrenia. Neurosci. Res. 62, 187–194.

Wakana, S., Jiang, H., Nagae-Poetscher, L.M., van Zijl, P.C., Mori, S., 2004. Fiber tract-based atlas of human white matter anatomy. Radiology 230, 77–87.

Yassa, M.A., Stark, C.E., 2009. A quantitative evaluation of cross-participant registration techniques for MRI studies of the medial temporal lobe. NeuroImage 44, 319–327.

Journal of Psychiatric Research 47 (2013) 1383–1388

Contents lists available at SciVerse ScienceDirect

Journal of Psychiatric Research

journal homepage: www.elsevier.com/locate/psychires

Discrimination between schizophrenia and major depressive disorder by magnetic resonance imaging of the female brain

Miho Ota [a,*], Masanori Ishikawa [b], Noriko Sato [c], Hiroaki Hori [a], Daimei Sasayama [a], Kotaro Hattori [a], Toshiya Teraishi [a], Takamasa Noda [a], Satoko Obu [a], Yasuhiro Nakata [a], Teruhiko Higuchi [a], Hiroshi Kunugi [a]

[a] Department of Mental Disorder Research, National Institute of Neuroscience, National Center of Neurology and Psychiatry, 4-1-1, Ogawa-Higashi, Kodaira, Tokyo 187-8502, Japan
[b] Department of Psychiatry, National Center Hospital of Neurology and Psychiatry, 4-1-1, Ogawa-Higashi, Kodaira, Tokyo 187-8551, Japan
[c] Department of Radiology, National Center Hospital of Neurology and Psychiatry, 4-1-1, Ogawa-Higashi, Kodaira, Tokyo 187-8551, Japan

ARTICLE INFO

Article history:
Received 25 February 2013
Received in revised form
14 June 2013
Accepted 14 June 2013

Keywords:
Diffusion tensor imaging
Discriminant analysis
Major depressive disorder
Magnetic resonance imaging
Schizophrenia

ABSTRACT

Background: Although schizophrenia and major depressive disorder (MDD) differ on a variety of neuroanatomical measures, a diagnostic tool to discriminate these disorders has not yet been established. We tried to identify structural changes of the brain that best discriminate between schizophrenia and MDD on the basis of gray matter volume, ventricle volume, and diffusion tensor imaging (DTI).
Method: The first exploration sample consisted of 25 female patients with schizophrenia and 25 females with MDD. Regional brain volumes and fractional anisotropy (FA) values were entered into a discriminant analysis. The second validation sample consisted of 18 female schizophrenia and 16 female MDD patients.
Results: The stepwise discriminant analysis resulted in correct classification rates of 0.80 in the schizophrenic group and 0.76 in MDD. In the second validation sample, the obtained model yielded correct classification rates of 0.72 in the schizophrenia group and 0.88 in the MDD group.
Conclusion: Our results suggest that schizophrenia and MDD have differential structural changes in the examined brain regions and that the obtained discriminant score may be useful to discriminate the two disorders.

1. Introduction

Major depressive disorder (MDD) is a common disorder with a lifetime prevalence reported to range from 8% to 12% in almost every country worldwide (Andrade et al., 2003). Schizophrenia is also common and reported to be ranged from 0.16% to 1.21% (Saha et al., 2005). Depression manifested in 21% to 74% of acute patients with recent onset schizophrenia and in 13% to 50% of those with chronic schizophrenia, while depressive features were found in even greater rates, up to 80%, in schizophrenia (Kollias et al., 2008). These data indicate that discrimination between schizophrenia and MDD is often difficult in the clinical setting.

Many magnetic resonance imaging (MRI) and diffusion tensor imaging (DTI) studies have focused on structural brain abnormalities in schizophrenia and MDD. In schizophrenia, evidence has been obtained showing changes in the frontal and temporal lobes, thalamus, anterior cingulate cortex (ACC), and corpus callosum, and showing dilatation of the Sylvian fissure and the third ventricle (reviewed by Arnone et al., 2009; Glahn et al., 2008; Honea et al., 2005; White et al., 2008). In MDD, changes in the frontal and temporal lobes, cingulum, and the subcortical structures have been reported (Arnone et al., 2012; Bora et al., 2012; Sexton et al., 2009).

Some studies have attempted to discriminate between patients with schizophrenia and healthy subjects using brain anatomical structures obtained by MRI (Leonard et al., 1999; Nakamura et al., 2007; Takayanagi et al., 2010). Other studies including ours reported an unbiased, rater-independent technique known as the voxel-based morphometry (VBM)-based classification approach (Davatzikos et al., 2005; Kawasaki et al., 2007; Ota et al., 2012). Each of these studies showed a fair to excellent classification rate. Additionally, one study evaluated the effectiveness of the structural neuroanatomy derived from MRI images as a diagnostic marker of MDD, and showed a relatively low classification rate (Costafreda et al., 2009). However, to our knowledge, there has been no

* Corresponding author. Tel.: +81 42 341 2711; fax: +81 42 346 2094.
E-mail address: ota@ncnp.go.jp (M. Ota).

0022-3956/$ – see front matter © 2013 Elsevier Ltd. All rights reserved.
http://dx.doi.org/10.1016/j.jpsychires.2013.06.010

attempt to produce an MRI-based diagnostic tool to objectively discriminate between schizophrenia and MDD.

Functional MRI and DTI have revealed the fine neural networks in the central nervous system (CNS). Together the thalamus, insula, ACC, and corpus callosum are regarded as the central relay station in the brain, and they can be subdivided into functionally different clusters (Buchsbaum et al., 1996; Makris et al., 2006; McCormick et al., 2006; Witelson, 1989). Several studies have detected subdivided region-specific brain changes for schizophrenia and MDD (Buchsbaum et al., 1996; Coryell et al., 2005; Crespo-Facorro et al., 2000; Makris et al., 2006; Mitelman et al., 2009). However, previous neuroimaging studies conducted to discriminate between schizophrenia and control and between MDD and controls paid little attention to these divisions. Moreover, the robust change of the ventricle size was known to be useful to distinguish the bipolar patients from schizophrenia patients (reviewed by Arnone et al., 2009). Then, it would be suitable to add the ventricles for variables of discriminant analysis between MDD and schizophrenia.

We hypothesized that the characteristic distribution of regional brain changes, especially in the limbic system and ventricles, in schizophrenia patients could have diagnostic value in that it could be used to discriminate individuals with schizophrenia from those with MDD.

2. Methods

2.1. Participants

The analysis proceeded in two stages. The first analysis was conducted to produce a statistical model to classify subjects according to the current diagnostic system, and the second analysis was performed to validate the statistical model by classifying a new cohort.

Toward this end, subjects were assigned to two independent groups based on the timing of their participation. The first exploration sample consisted of 25 patients with schizophrenia and 25 with MDD. Consensus diagnosis by at least two psychiatrists was made according to the Diagnostic and Statistical Manual of Mental Disorders, 4th edition (DSM-IV) (American Psychiatric Association 1994). The second validation sample consisted of 18 patients with schizophrenia and 16 with MDD. All subjects were Japanese females and biologically unrelated to each other. Exclusion criteria included a history of head injury, central nerve system disease, speech or hearing difficulties, significant cerebrovascular diseases (cortical infarctions, multiple lacunar lesions or leukoaraiosis), and fulfillment of the DSM-IV criteria for abuse of illicit drugs or alcohol at any point during their lifetime. Further, to avoid the co-morbidity of the psychiatric illness, the schizophrenic patients treated with antidepressants were excluded from the study. The psychopathological state of all of the schizophrenia subjects was assessed with the Positive and Negative Syndrome Scale (PANSS; Kay et al., 1987), and the patients with MDD were rated with the Hamilton Depression Rating Scale (HAM-D) (Hamilton, 1960) for their depressive symptoms. Daily doses of antipsychotics including depot antipsychotics and antidepressants were converted to chlorpromazine and imipramine equivalents, respectively using published guidelines (American Psychiatric Association 1997; Inagaki et al. 1999). The study protocol was approved by the ethics committee of the National Center of Neurology and Psychiatry, Japan, and written informed consent for participation in the study was obtained from all subjects.

2.2. MRI data acquisition and processing

MR studies were performed on a Magnetom Symphony 1.5-tesla (Siemens, Erlangen, Germany). Three-dimensional (3D) T1-weighted images were scanned in the sagittal plane (echo time [TE]/repetition time [TR], 2.64/1580 ms; flip angle, 15 degrees; slab thickness, 177 mm; matrix, 208 × 256; number of excitations [NEX] = 1, field of view [FOV], 256 × 315 mm^2; slice thickness, 1.23 mm) yielding 144 contiguous slices through the head. The raw 3D T1-weighted volume data were transferred to a workstation, and structural images were analyzed using Statistical Parametric Mapping 8 (SPM8) software (Wellcome Department of Imaging Neuroscience, London, UK) running on MATLAB 7.0 (Math Works, Natick, MA). First, each individual 3D-T1 image was normalized with the diffeomorphic anatomical registration using exponentiated lie (DARTEL) registration method (Ashburner 2007). Normalized segmented images were modulated by multiplication with Jacobian determinants of the spatial normalization function to encode the deformation field for each subject as tissue density changes in normal space. Gray matter volume images and the cerebrospinal fluid (CSF) images were smoothed using a 12-mm full-width at half-maximum of an isotropic Gaussian kernel.

DTI was performed in the axial plane (TE/TR, 106/11, 200 ms; FOV, 240 × 240 mm^2; matrix, 96 × 96; 75 continuous transverse slices; slice thickness 2.5 mm with no interslice gap). To enhance the signal-to-noise ratio, acquisition was repeated two times. Diffusion was measured along 12 noncollinear directions using a diffusion-weighted factor b in each direction for 1000 s/mm^2, and one image was acquired without using any diffusion gradient. The DTI data sets were analyzed using the DtiStudio program (Jiang et al., 2006). The diffusion tensor parameters were calculated on a pixel-by-pixel basis, and the FA and $b = 0$ image were calculated according to Wakana et al. (2004). FA images were normalized to the standard space. First, each individual 3D-T1 image was coregistered and resliced to its own $b = 0$ image. Next, the coregistered 3D-T1 image was normalized with the DARTEL registration method using SPM8. Finally, the transformation matrix was applied to the FA map. Each map was then spatially smoothed with a 6-mm full-width at half-maximum Gaussian kernel in order to decrease spatial noise and compensate for the inexactitude of normalization.

2.3. Regions of interest

The insula was divided into anterior and posterior parts (Fig. 1a), the thalamus into five subregions (Fig. 1b), the ACC into four subregions (Fig. 1c), and the corpus callosum into six subregions (Fig. 1d). The detailed descriptions of these subregions are given in the Supplementary Information. The Regions of interest (ROIs) of 3rd, 4th, and lateral ventricle were derived from the WFU_pickatlas, extension program of SPM8 (Maldjian et al., 2003, 2004). ROIs were operationally defined on the standard brain of the SPM8, "avg152T1.nii" image. FA values, gray matter volume and ventricle size were both calculated for these ROIs. The boundaries of these ROIs were manually determined using MRIcro (Chris Rorden, University of Nottingham, Nottingham, Great Britain).

2.4. Statistical analysis

Discriminant function analyses were conducted to assess the ability of combinations of brain anatomical variables to distinguish between patients with schizophrenia and those with MDD. The independent variables were the regional gray matter and ventricle volumes/whole brain volume and FA values derived from each normalized individual image by the ROI method using the software MarsBar (Brett et al., 2002). We regarded the gray matter volume plus white matter volume as the whole brain volume. The values of gray and white matter volumes of individual subjects were extracted with the Easy Volume toolbox (http://www.sbirc.ed.ac.uk/LCL/LCL_M1.html) (Pernet et al., 2009) running on Matlab 7.0.

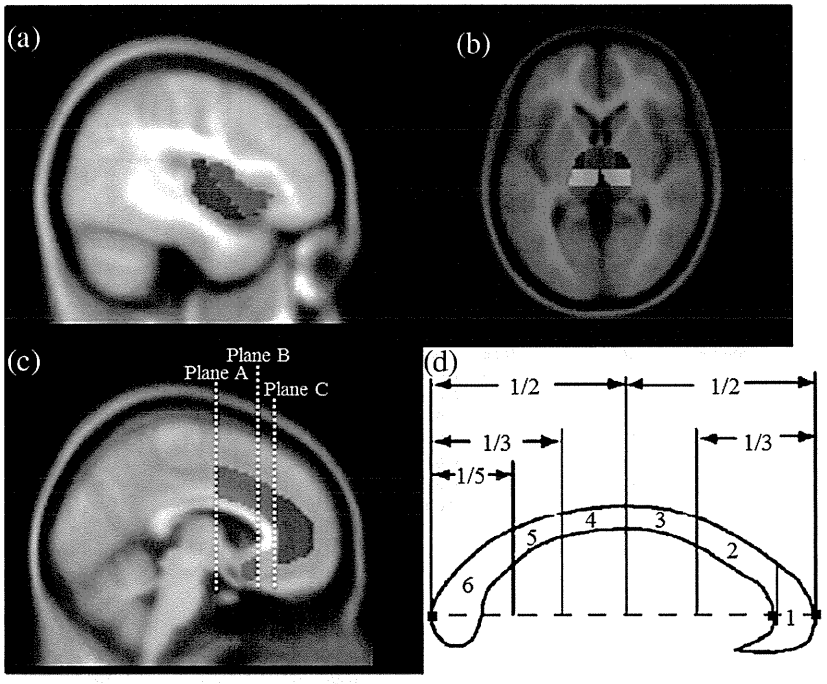

Fig. 1. The subclassification of the regions of interest (ROIs). (a) The insula was divided into two subregions: anterior (pink) and posterior (green). (b) The thalamus was divided into five subregions; the medial portions of the anterior (light blue) and central (purple) divisions, the lateral portions of the anterior (pink) and central divisions (green), and posterior divisions (red-orange). (c) The ACC was divided into four subregions; dorsal (red), rostral (blue), subcallosal (green), and subgenual subregions (pink). (d) Perpendiculars to this axis were drawn at specific arithmetic divisions, resulting in six callosal segments. The corpus callosum was divided into six subregions: genu (1), rostral body (2), anterior midbody (3), posterior midbody (4), isthmus (5) and splenium (6).

We entered FA values in bilateral anterior and posterior insulae, five thalamic subregions, four regions of the ACC, and six subregions of the corpus callosum, and volume data in bilateral anterior and posterior insulae, five thalamic subregions, and four anterior cingulate subregions, 3rd, 4th, and lateral ventricles as variables.

Discriminant functions were derived by stepwise methods after Wilks' method. The test was performed with the SPSS software ver. 17 (SPSS Japan, Tokyo). The stepwise selection criteria were determined by the overall multivariate *F*-value of each variable to test the differences between the patients with schizophrenia and those with MDD and to maximize the discriminant function between the groups. The enter-criterion was $F = 5$, and the remove-criterion was $F = 4$. An analysis was then performed to prospectively validate the statistical model, the linear discriminant function analysis, by successfully classifying the first two-group sample.

3. Results

The demographic and clinical data of the subjects are shown in Table 1, and the mean regional volumes and FA values of each ROIs were described in Table 2. The differences between the patients with schizophrenia and MDD were analyzed by two sample *t*-test. There was no significant difference in age, years of education, or whole brain volume between the schizophrenia and MDD groups in either sample.

Table 1
Demographic and clinical characteristics of the subjects.

Variable	(a) Exploration sample			(b) Validation sample		
	Schizophrenia	Major Depressive Disorder	*p* value	Schizophrenia	Major Depressive Disorder	*p* value
	Female ($n = 25$)	Female ($n = 25$)		Female ($n = 18$)	Female ($n = 16$)	
	Mean ± SD	Mean ± SD		Mean ± SD	Mean ± SD	
Age (years)	40.3 ± 10.6	42.3 ± 9.4	0.48	37.0 ± 8.7	41.5 ± 10.5	0.12
Education (years)	13.7 ± 2.5	14.5 ± 1.9	0.20	14.8 ± 2.5	14.5 ± 2.1	0.89
Duratin of illness (year)	17.9 ± 9.8	9.1 ± 9.1	0.002	15.6 ± 8.9	7.1 ± 5.9	0.012
Whole brain volume (liter)	1.10 ± 0.08	1.08 ± 0.08	0.42	1.13 ± 0.10	1.08 ± 0.10	0.20
Antipsychotic medication*	654.3 ± 547.1	8.0 ± 40.0	<0.001	427.0 ± 483.4	56.3 ± 225.0	0.006
Antidepressant medication#	0.0 ± 0.0	105.4 ± 143.0	0.001	0.0 ± 0.0	99.8 ± 103.1	0.001
Number of hospitalizations	3.5 ± 4.5	0.3 ± 0.5	0.002	1.8 ± 2.3	0.6 ± 1.0	0.023
HAM-D		12.2 ± 8.3			11.9 ± 7.2	
PANSS positive	14.6 ± 5.9			15.4 ± 6.1		
PANSS negative	16.8 ± 8.4			14.1 ± 4.8		
PANSS general	32.4 ± 13.5			29.6 ± 7.3		

HAM-D: Hamilton's rating scale for depression; PANSS: positive and negative syndrome scale; SD: standard deviation.
*: Chlorpromazine equivalent. #: Imipramine equivalent.

Table 2
Mean regional volume and fractional anisotropy of the subjects.

Region	Modality	Laterality	(a) Exploration sample			(b) Validation sample		
			Schizophrenia	MDD	*p* value	Schizophrenia	MDD	*p* value
			Mean ± SD	Mean ± SD		Mean ± SD	Mean ± SD	
Corpus callosum 1	FA		0.49 ± 0.04	0.48 ± 0.04	0.52	0.51 ± 0.03	0.49 ± 0.04	0.09
Corpus callosum 2	FA		0.47 ± 0.05	0.49 ± 0.04	0.21	0.50 ± 0.05	0.50 ± 0.03	0.61
Corpus callosum 3	FA		0.43 ± 0.04	0.44 ± 0.04	0.37	0.45 ± 0.05	0.45 ± 0.04	0.69
Corpus callosum 4	FA		0.42 ± 0.04	0.42 ± 0.05	0.98	0.43 ± 0.05	0.42 ± 0.03	0.57
Corpus callosum 5	FA		0.43 ± 0.04	0.44 ± 0.05	0.32	0.45 ± 0.04	0.44 ± 0.03	0.55
Corpus callosum 6	FA		0.54 ± 0.03	0.55 ± 0.02	0.66	0.56 ± 0.03	0.56 ± 0.02	0.61
Anterior insula	FA	Left	0.22 ± 0.01	0.21 ± 0.01	0.04	0.21 ± 0.01	0.21 ± 0.01	0.91
		Right	0.21 ± 0.01	0.20 ± 0.01	0.03	0.20 ± 0.01	0.20 ± 0.01	0.92
	Volume	Left	0.38 ± 0.02	0.40 ± 0.03	0.05	0.37 ± 0.03	0.39 ± 0.02	0.06
		Right	0.39 ± 0.03	0.41 ± 0.03	0.01	0.38 ± 0.03	0.40 ± 0.03	0.05
Posterior insula	FA	Left	0.24 ± 0.02	0.23 ± 0.01	0.13	0.24 ± 0.01	0.23 ± 0.01	0.78
		Right	0.22 ± 0.01	0.22 ± 0.01	0.25	0.22 ± 0.01	0.22 ± 0.01	0.58
	Volume	Left	0.35 ± 0.03	0.36 ± 0.02	0.13	0.35 ± 0.02	0.36 ± 0.02	0.24
		Right	0.37 ± 0.03	0.37 ± 0.02	0.44	0.36 ± 0.02	0.37 ± 0.02	0.03
Anterolateral region of thalamus	FA	Left	0.46 ± 0.02	0.46 ± 0.02	0.22	0.46 ± 0.02	0.45 ± 0.02	0.07
		Right	0.46 ± 0.02	0.46 ± 0.02	0.88	0.46 ± 0.02	0.46 ± 0.02	0.56
	Volume	Left	0.09 ± 0.01	0.09 ± 0.01	0.41	0.08 ± 0.01	0.09 ± 0.01	0.01
		Right	0.09 ± 0.01	0.09 ± 0.01	0.32	0.09 ± 0.01	0.10 ± 0.01	0.00
Antero medial region of thalamus	FA	Left	0.32 ± 0.02	0.33 ± 0.02	0.59	0.33 ± 0.02	0.32 ± 0.02	0.20
		Right	0.32 ± 0.01	0.32 ± 0.02	0.75	0.34 ± 0.02	0.33 ± 0.02	0.31
	Volume	Left	0.22 ± 0.02	0.22 ± 0.02	0.29	0.21 ± 0.02	0.23 ± 0.03	0.00
		Right	0.23 ± 0.02	0.24 ± 0.02	0.03	0.22 ± 0.02	0.25 ± 0.03	0.00
Central lateral region of thalamus	FA	Left	0.41 ± 0.02	0.41 ± 0.02	0.56	0.41 ± 0.02	0.41 ± 0.02	0.75
		Right	0.40 ± 0.02	0.40 ± 0.02	0.81	0.40 ± 0.01	0.40 ± 0.02	0.49
	Volume	Left	0.14 ± 0.02	0.14 ± 0.01	0.66	0.13 ± 0.01	0.14 ± 0.01	0.02
		Right	0.17 ± 0.02	0.17 ± 0.01	0.45	0.17 ± 0.01	0.18 ± 0.02	0.02
Central medial region of thalamus	FA	Left	0.27 ± 0.02	0.28 ± 0.02	0.28	0.28 ± 0.02	0.27 ± 0.02	0.14
		Right	0.27 ± 0.02	0.27 ± 0.02	0.93	0.28 ± 0.02	0.27 ± 0.02	0.14
	Volume	Left	0.25 ± 0.02	0.26 ± 0.02	0.21	0.25 ± 0.02	0.27 ± 0.03	0.06
		Right	0.27 ± 0.02	0.28 ± 0.02	0.11	0.27 ± 0.02	0.29 ± 0.03	0.01
Posterior region of thalamus	FA	Left	0.27 ± 0.02	0.28 ± 0.02	0.08	0.28 ± 0.02	0.28 ± 0.01	0.89
		Right	0.27 ± 0.02	0.28 ± 0.02	0.10	0.28 ± 0.02	0.28 ± 0.01	0.84
	Volume	Left	0.22 ± 0.02	0.23 ± 0.02	0.46	0.22 ± 0.01	0.23 ± 0.02	0.06
		Right	0.25 ± 0.02	0.25 ± 0.02	0.80	0.24 ± 0.01	0.25 ± 0.02	0.03
Dorsoral ACC	FA	Left	0.26 ± 0.01	0.25 ± 0.01	0.19	0.25 ± 0.01	0.25 ± 0.01	0.73
		Right	0.31 ± 0.01	0.31 ± 0.01	0.75	0.31 ± 0.01	0.31 ± 0.01	0.53
	Volume	Left	0.37 ± 0.02	0.37 ± 0.02	0.17	0.37 ± 0.03	0.37 ± 0.02	0.69
		Right	0.32 ± 0.02	0.32 ± 0.02	0.56	0.32 ± 0.02	0.32 ± 0.02	0.90
Rostral ACC	FA	Left	0.19 ± 0.01	0.19 ± 0.01	0.23	0.19 ± 0.01	0.18 ± 0.01	0.04
		Right	0.24 ± 0.01	0.24 ± 0.01	0.16	0.24 ± 0.01	0.23 ± 0.01	0.32
	Volume	Left	0.41 ± 0.03	0.42 ± 0.03	0.41	0.42 ± 0.03	0.42 ± 0.02	0.84
		Right	0.38 ± 0.03	0.38 ± 0.03	0.35	0.38 ± 0.03	0.39 ± 0.02	0.31
Subcallosal ACC	FA	Left	0.22 ± 0.02	0.22 ± 0.02	0.93	0.22 ± 0.01	0.22 ± 0.02	0.26
		Right	0.29 ± 0.02	0.26 ± 0.02	0.00	0.28 ± 0.02	0.26 ± 0.03	0.01
	Volume	Left	0.40 ± 0.03	0.40 ± 0.03	0.36	0.39 ± 0.03	0.40 ± 0.03	0.25
		Right	0.35 ± 0.03	0.36 ± 0.03	0.28	0.36 ± 0.03	0.36 ± 0.03	0.48
Subgenual ACC	FA	Left	0.20 ± 0.02	0.21 ± 0.02	0.31	0.21 ± 0.02	0.20 ± 0.01	0.58
		Right	0.25 ± 0.03	0.24 ± 0.02	0.32	0.24 ± 0.02	0.24 ± 0.02	0.68
	Volume	Left	0.40 ± 0.03	0.41 ± 0.03	0.18	0.38 ± 0.03	0.40 ± 0.03	0.06
		Right	0.41 ± 0.02	0.42 ± 0.03	0.11	0.39 ± 0.03	0.41 ± 0.03	0.12
3rd ventricle	Volume		0.19 ± 0.05	0.17 ± 0.03	0.28	0.18 ± 0.04	0.18 ± 0.04	0.72
4th ventricle	Volume		0.18 ± 0.04	0.17 ± 0.03	0.27	0.18 ± 0.05	0.18 ± 0.05	0.99
Lateral ventricle	Volume		0.21 ± 0.12	0.19 ± 0.07	0.51	0.17 ± 0.07	0.18 ± 0.05	0.51

FA: fractional anisotropy; ACC: anterior cingulate cortex; MDD: major depressive disorder.

The stepwise discriminant analysis yielded a model in which three variables were selected. The obtained equation to calculate "discriminant score" is:

$$\text{Discriminant score} = 46.0 \times x - 39.4 \times y - 36.8 \times z + 6.9$$

where x is the FA value in the right subcallosal cingulate, y is the FA value in the posterior subregion of the thalamus, and z is the ratio of gray matter volume/whole brain volume in the right medial portion of the anterior thalamus. When the discriminant score is >0, it predicts that the patient has schizophrenia, and scores <0 predict MDD.

The use of these variables resulted in correct classification rates of 0.80 in schizophrenic patients and 0.76 in MDD patients in the first sample ($\chi^2 = 27.8$; df = 3; $p < 0.001$; Wilks' lambda = 0.55) (Fig. 2a). When the obtained discriminant model was applied to the second sample, the correct classification rates were 0.72 in schizophrenia and 0.88 in MDD groups (Fig. 2b).

4. Discussion

To our knowledge, this is the first attempt to produce a diagnostic tool to discriminate between schizophrenia and MDD based on structural MRI of the brain. Among the 31 ROIs located in the

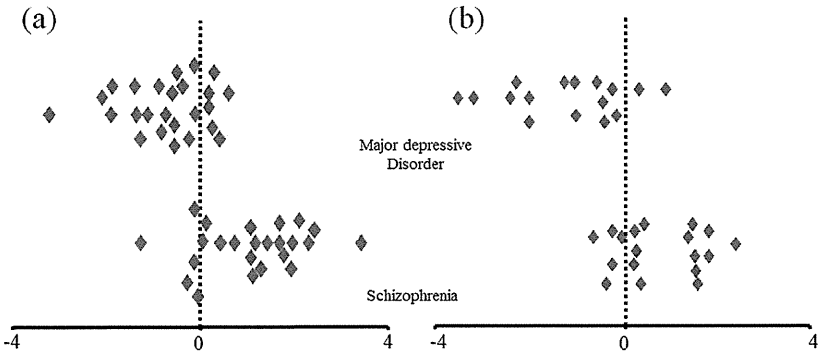

Fig. 2. Plot of discriminant scores in schizophrenic and MDD patients. (a) Discriminant scores of 25 schizophrenia patients and 25 MDD patients. (b) Discriminant scores of the second cohort of 18 schizophrenia patients and 16 MDD patients based on a linear discriminant function analysis between the original comparison samples.

thalami, ACC, insulae, corpus callosum, 3rd, 4th and lateral ventricles, three ROIs (i.e., the right subcallosal ACC, posterior subregion of the thalamus, and right medial portion of the anterior thalamus.) were selected to produce the discriminant model by the stepwise method. As for the correct classification rates, our results showed good classification rates of schizophrenia (0.80) and MDD (0.76) in the first exploration sample (0.90–1.00 = "excellent", 0.80–0.89 = "good", 0.70–0.79 = "fair", 0.60–0.69 = "poor", and 0.50–0.59 = "fail", according to Hanley and McNeil (1982) and Lasko et al. (2005)). Importantly, this discriminant model successfully classified the second sample of schizophrenia (0.72; fair), and MDD (0.88; good).

Several studies used high-resolution structural MRI scans as inputs to classification algorithms to distinguish between patients with schizophrenia and healthy volunteers, with reported accuracies ranging from 79% to 94% (Csernansky et al., 2004; Davatzikos et al., 2005; Fan et al., 2005; Kawasaki et al., 2007; Yoon et al., 2007). A few studies have assessed the feasibility of using FA and/or mean diffusivity (MD) maps in conjunction with automatic pattern recognition methods to differentiate between the two groups, and they correctly classified the patients with 75–94% accuracy (Ardekani et al., 2011; Caan et al., 2006; Caprihan et al., 2008).

Further, the accuracy of the structural neuroanatomy such as right subcallosal ACC and precuneus as a diagnostic marker for MDD was 67.6% (Costafreda et al., 2009). The relatively low accuracy rate in our study may have occurred because patients with mood disorders tend to share some neuroanatomical changes with schizophrenic patients (e.g. Meisenzahl et al., 2010).

The discriminant model in this study included the gray matter volume in the right medial portions of the anterior thalamus and FA in the right posterior subregion of the thalamus; these regions have been well known to be affected in schizophrenia, but not MDD (Honea et al., 2005; Konick and Friedman, 2001). On the other hand, previous neuroimaging studies showed the volume reduction of the subcallosal ACC in cases of MDD (Coryell et al., 2005; Costafreda et al., 2009; Pezawas et al., 2005). The discriminant model in this study also employed FA in the right subcallosal cingulate as a positive coefficient, and this is compatible with the preceding ones.

Limitation of the present study must be taken into account. First, this study included only female subjects. It is known that there were gender differences in brain morphology reported in MDD as well as schizophrenia patients (Suzuki et al., 2002; Takahashi et al., 2010), and that gender-difference effects on the course of progressive brain change in schizophrenia (Irle et al., 2011). In addition, some papers detect the gender-difference of brain configuration and the aging effect on the brain (Good et al., 2001; Pruessner et al., 2001). The correlative brain changes in male subjects need to be investigated separately. Second, there was a difference of mean duration of illness between the patient groups and we did not adjust the potential effects of age and duration of illness. It has been suggested that in schizophrenic patients, progressive brain changes occur that are rapid and diffuse compared with the aging effect of healthy subjects (Friedman et al., 2008; Mori et al., 2007). The effects of degenerative factors on the brain with MDD are not yet understood, and it is difficult to specify the duration of illness in MDD patient because MDD follows relapsing-remitting course. There is a need for systematic studies. It is difficult to adjust the factors that have different effects on the two groups respectively, so we tried to cope with these factors by balancing the mean age of the diagnostic groups.

In conclusion, our results suggest that schizophrenia and MDD have differential structural changes in the brain regions examined herein, and that a combination of such differences is useful to discriminate between patients with schizophrenia and those with MDD.

Role of funding sources

This study was supported by Health and Labor Sciences Research Grants (Comprehensive Research on Disability, Health, and Welfare) (M.O. and H.K.), Intramural Research Grant (24-11) for Neurological and Psychiatric Disorders of NCNP (M.O. and H.K.), "Understanding of molecular and environmental bases for brain health" carried out under the Strategic Research Program for Brain Sciences by the Ministry of Education, Culture, Sports, Science and Technology of Japan (H.K.).

Contributors

Miho Ota designed the study and wrote the first draft of the manuscript. Masanori Ishikawa collected data. Noriko Sato managed the analyses. Hiroaki Hori collected data. Daimei Sasayama collected data. Kotaro Hattori collected data. Toshiya Teraishi collected data. Takamasa Noda collected data. Satoko Obu collected data. Yasuhiro Nakata collected data. Teruhiko Higuchi managed the analyses. Hiroshi Kunugi managed the analyses. All authors contributed to and have approved the final manuscript.

Conflict of interest

All authors declare that they have no conflicts of interest.

Appendix A. Supplementary data

Supplementary data related to this article can be found at http://dx.doi.org/10.1016/j.jpsychires.2013.06.010.

References

American Psychiatric Association. DSM-IV Diagnostic and Statistical Manual of Mental Disorders. 4th ed. Washington, DC: APA; 1994.

American Psychiatric Association. Practice Guidelines for the Treatment of Patients with Schizophrenia. Washington, DC: American Psychiatric Press; 1997.

Andrade L, Caraveo-Anduaga JJ, Berglund P, Bijl RV, De Graaf R, Vollebergh W, et al. The epidemiology of major depressive episodes: results from the International Consortium of Psychiatric Epidemiology (ICPE) Surveys. International Journal of Methods in Psychiatric Research 2003;12(1):3–21.

Ardekani BA, Tabesh A, Sevy S, Robinson DG, Bilder RM, Szeszko PR. Diffusion tensor imaging reliably differentiates patients with schizophrenia from healthy volunteers. Human Brain Mapping 2011;32(1):1–9.

Arnone D, Cavanagh J, Gerber D, Lawrie SM, Ebmeier KP, McIntosh AM. Magnetic resonance imaging studies in bipolar disorder and schizophrenia: meta-analysis. British Journal of Psychiatry 2009;195(3):194–201.

Arnone D, McIntosh AM, Ebmeier KP, Munaf MR, Anderson IM. Magnetic resonance imaging studies in unipolar depression: systematic review and meta-regression analyses. European Neuropsychopharmacology 2012;22(1):1–16.

Ashburner J. A fast diffeomorphic image registration algorithm. Neuroimage 2007;38(1):95–113.

Bora E, Harrison BJ, Davey CG, Yücel M, Pantelis C. Meta-analysis of volumetric abnormalities in cortico-striatal-pallidal-thalamic circuits in major depressive disorder. Psychological Medicine 2012;42(4):671–81.

Brett, M., Anton, J.L., Valabregue, R., Poline, J.B., 2002. Region of interest analysis using an SPM toolbox [Abstract] presented at the 8th International Conference on Functional Mapping of the Human Brain. June 2–6, Sendai, Japan. Available on CD-ROM in Neuroimage, vol. 16, No. 2.

Buchsbaum MS, Someya T, Teng CY, Abel L, Chin S, Najafi A, et al. PET and MRI of the thalamus in never-medicated patients with schizophrenia. American Journal of Psychiatry 1996;153(2):191–9.

Caan MWA, Vermeer KA, van Vliet LJ, Majoie CBLM, Peters BD, den Heeten GJ, et al. Shaving diffusion tensor images in discriminant analysis: a study into schizophrenia. Medical Image Analysis 2006;10(6):841–9.

Caprihan A, Pearlson GD, Calhoun VD. Application of principal component analysis to distinguish patients with schizophrenia from healthy controls based on fractional anisotropy measurements. Neuroimage 2008;42(2):675–82.

Coryell W, Nopoulos P, Drevets W, Wilson T, Andreasen NC. Subgenual prefrontal cortex volumes in major depressive disorder and schizophrenia: diagnostic specificity and prognostic implications. American Journal of Psychiatry 2005;162(9):1706–17012.

Costafreda SG, Chu C, Ashburner J, Fu CH. Prognostic and diagnostic potential of the structural neuroanatomy of depression. PLoS One 2009;4(7):e6353.

Crespo-Facorro B, Kim JJ, Andreasen NC, O'Leary DS, Bockholt J, Magnotta V. Insular cortex abnormalities in schizophrenia: a structural magnetic resonance imaging study of first-episode patients. Schizophrenia Research 2000;46(1):35–43.

Csernansky JG, Schindler MK, Splinter NR, Wang L, Gado M, Selemon LD, et al. Abnormalities of thalamic volume and shape in schizophrenia. American Journal of Psychiatry 2004;161(5):896–902.

Davatzikos C, Shen D, Gur RC, Wu X, Liu D, Fan Y, et al. Whole-brain morphometric study of schizophrenia revealing a spatially complex set of focal abnormalities. Archives of General Psychiatry 2005;62(11):1218–27.

Fan Y, Shen D, Davatzikos C. Classification of structural images via high-dimensional image warping, robust feature extraction, and SVM. Medical Image Computing and Computer-Assisted Intervention 2005;Pt 1:1–8.

Friedman JI, Tang C, Carpenter D, Buchsbaum M, Schmeidler J, Flanagan L, et al. Diffusion tensor imaging findings in first-episode and chronic schizophrenia patients. American Journal of Psychiatry 2008;165(8):1024–32.

Glahn DC, Laird AR, Ellison-Wright I, Thelen SM, Robinson JL, Lancaster JL, et al. Meta-analysis of gray matter anomalies in schizophrenia: application of anatomic likelihood estimation and network analysis. Biological Psychiatry 2008;64(9):774–81.

Good CD, Johnsrude I, Ashburner J, Henson RNA, Friston KJ, Frackowiak RSJ. Cerebral asymmetry and the effect of sex and handedness on brain structure: a voxel-based morphometric analysis of 465 normal adult human brains. Neuroimage 2001;14(3):685–700.

Hamilton M. A rating scale of depression. Journal of Neurology, Neurosurgery and Psychiatry 1960;23(1):56–62.

Hanley J, McNeil B. The meaning and use of the area under a receiver operating characteristic (ROC) curve. Radiology 1982;143(1):29–36.

Honea R, Crow TJ, Passingham D, Mackay CE. Regional deficits in brain volume in schizophrenia: a meta-analysis of voxel-based morphometry studies. American Journal of Psychiatry 2005;162(12):2233–45.

Inagaki A, Inada T, Fujii Y, Yagi G. Equivalent dose of psychotropics. Tokyo: Seiwa Shoten; 1999.

Irle E, Lange C, Ruhleder M, Exner C, Siemerkus J, Weniger G. Hippocampal size in women but not men with schizophrenia relates to disorder duration. Psychiatry Research 2011;192(3):133–9.

Jiang H, van Zijil PC, Kim J, Pearlson GD, Mori S. DtiStudio: resource program for diffusion tensor computation and fiber bundle tracking. Computer Methods and Programs in Biomedicine 2006;81(2):106–16.

Kawasaki Y, Suzuki M, Kherif F, Takahashi T, Zhou SY, Nakamura K, et al. Multivariate voxel-based morphometry successfully differentiates schizophrenia patients from healthy controls. Neuroimage 2007;34(1):235–42.

Kay SR, Opler LA, Fiszbein A. Positive and Negative Syndrome Scale (PANSS) manual. Schizophrenia Bulletin 1987;13(2):261–76.

Kollias CT, Kontaxakis VP, Havaki-Kontaxaki BJ, Stamouli S, Margariti M, Petridou E. Association of physical and social anhedonia with depression in the acute phase of schizophrenia. Psychopathology 2008;41(6):365–70.

Konick LC, Friedman L. Meta-analysis of thalamic size in schizophrenia. Biological Psychiatry 2001;49(1):28–38.

Lasko T, Bhagwat J, Zou K, Ohno-Machado L. The use of receiver operating characteristic curves in biomedical informatics. Journal of Biomedical Informatics 2005;38(5):404–15.

Leonard CM, Kuldau JM, Breier JI, Zuffante PA, Gautier ER, Heron DC, et al. Cumulative effect of anatomical risk factors for schizophrenia: an MRI study. Biological Psychiatry 1999;46(3):374–82.

Makris N, Goldstein J, Kennedy D, Hodge S, Caviness V, Faraone S, et al. Decreased volume of left and total anterior insular lobule in schizophrenia. Schizophrenia Research 2006;83(2-3):155–71.

Maldjian JA, Laurienti PJ, Kraft RA, Burdette JH. An automated method for neuroanatomic and cytoarchitectonic atlas-based interrogation of fMRI data sets. Neuroimage 2003;19(3):1233–9.

Maldjian JA, Laurienti PJ, Burdette JH. Precentral gyrus discrepancy in electronic versions of the Talairach atlas. Neuroimage 2004;21(1):450–5.

McCormick LM, Ziebell S, Nopoulos P, Cassell M, Andreasen NC, Brumm M. Anterior cingulate cortex: an MRI-based parcellation method. Neuroimage 2006;32(3):1167–75.

Meisenzahl EM, Seifert D, Bottlender R, Teipel S, Zetzsche T, Jäger M, et al. Differences in hippocampal volume between major depression and schizophrenia: a comparative neuroimaging study. European Archives of Psychiatry and Clinical Neuroscience 2010;260(2):127–37.

Mitelman SA, Nikiforova YK, Canfield EL, Hazlett EA, Brickman AM, Shihabuddin L, et al. A longitudinal study of the corpus callosum in chronic schizophrenia. Schizophrenia Research 2009;114(1-3):144–53.

Mori T, Ohnishi T, Hashimoto R, Nemoto K, Moriguchi Y, Noguchi H, et al. Progressive changes of white matter integrity in schizophrenia revealed by diffusion tensor imaging. Psychiatry Research 2007;154:133–45.

Nakamura M, Salisbury DF, Hirayasu Y, Bouix S, Pohl KM, Yoshida T, et al. Neocortical gray matter volume in first-episode schizophrenia and first-episode affective psychosis: a cross-sectional and longitudinal MRI study. Biological Psychiatry 2007;62:773–83.

Ota M, Sato N, Ishikawa M, Hori H, Sasayama D, Hattori K, et al. Discrimination of schizophrenic females from healthy women using multiple structural brain measures obtained with voxel-based morphometry. Psychiatry and Clinical Neurosciences 2012;66(7):611–7.

Pruessner JC, Collins DL, Pruessner M, Evans AC. Age and gender predict volume decline in the anterior and posterior hippocampus in early adulthood. Journal of Neuroscience 2001;21(1):194–200.

Pernet C, Andersson J, Paulesu E, Demonet JF. When all hypotheses are right: a multifocal account of dyslexia. Human Brain Mapping 2009;30(7):2278–92.

Pezawas L, Meyer-Lindenberg A, Drabant EM, Verchinski BA, Munoz KE, Kolachana BS, et al. 5-HTTLPR polymorphism impacts human cingulate-amygdala interactions: a genetic susceptibility mechanism for depression. Nature Neuroscience 2005;8(6):828–34.

Saha S, Chant D, Welham J, McGrath J. A systematic review of the prevalence of schizophrenia. PLoS Medicine 2005;2(5):e141.

Sexton CE, Mackay CE, Ebmeier KP. A systematic review of diffusion tensor imaging studies in affective disorders. Biological Psychiatry 2009;66(9):814–23.

Suzuki M, Nohara S, Hagino H, Kurokawa K, Yotsutsuji T, Kawasaki Y, et al. Regional change in gray and white matter in patients with schizophrenia demonstrated with voxel-based analysis of MRI. Schizophrenia Research 2002;55(1-2):41–54.

Takahashi T, Yücel M, Lorenzetti V, Tanino R, Whittle S, Suzuki M, et al. Volumetric MRI study of the insular cortex in individuals with current and past major depression. Journal of Affective Disorders- 2010;121(3):231–8.

Takayanagi Y, Kawasaki Y, Nakamura K, Takahashi T, Orikabe L, Toyoda E, et al. Differentiation of first-episode schizophrenia patients from healthy controls using ROI-based multiple structural brain variables. Progress in Neuropsychopharmacology and Biological Psychiatry 2010;34(1):10–7.

Wakana S, Jiang H, Nagae-Poetscher LM, van Zijl PC, Mori S. Fiber tract-based atlas of human white matter anatomy. Radiology 2004;230(1):77–87.

White T, Nelson M, Lim KO. Diffusion tensor imaging in psychiatric disorders. Topics in Magnetic Resonance Imaging 2008;19(2):97–109.

Witelson SF. Hand and sex differences in the isthmus and genu of the human corpus callosum. Brain 1989;112(Pt 3):799–835.

Yoon U, Lee JM, Im K, Shin YW, Cho BH, Kim IY, et al. Pattern classification using principal components of cortical thickness and its discriminative pattern in schizophrenia. Neuroimage 2007;34(4):1405–15.

Schizophrenia Research xxx (2014) xxx–xxx

Contents lists available at ScienceDirect

Schizophrenia Research

journal homepage: www.elsevier.com/locate/schres

Pseudo-continuous arterial spin labeling MRI study of schizophrenic patients

Miho Ota [a,*], Masanori Ishikawa [b], Noriko Sato [c], Mitsutoshi Okazaki [b], Norihide Maikusa [d], Hiroaki Hori [a], Kotaro Hattori [a], Toshiya Teraishi [a], Kimiteru Ito [c], Hiroshi Kunugi [a]

[a] Department of Mental Disorder Research, National Institute of Neuroscience, National Center of Neurology and Psychiatry, 4-1-1, Ogawa-Higashi, Kodaira, Tokyo 187-8502, Japan
[b] Department of Psychiatry, National Center of Neurology and Psychiatry, 4-1-1, Ogawa-Higashi, Kodaira, Tokyo 187-8502, Japan
[c] Department of Radiology, National Center of Neurology and Psychiatry, 4-1-1, Ogawa-Higashi, Kodaira, Tokyo 187-8502, Japan
[d] Department of Imaging Neuroinformatics, Integrative Brain Imaging Center, National Center of Neurology and Psychiatry, 4-1-1, Ogawa-Higashi, Kodaira, Tokyo 187-8502, Japan

ARTICLE INFO

Article history:
Received 14 May 2013
Received in revised form 16 December 2013
Accepted 16 January 2014
Available online xxxx

Keywords:
Biological parametric mapping
Cerebral blood flow
Diffeomorphic anatomical registration using exponentiated Lie algebra
Pseudo-continuous arterial spin labeling
Schizophrenia
Tract-based spatial statistics

ABSTRACT

Arterial spin labeling (ASL) magnetic resonance imaging (MRI) is a novel noninvasive technique that can measure regional cerebral blood flow (rCBF). To our knowledge, few studies have examined rCBF in patients with schizophrenia by ASL-MRI. Here we used pseudo-continuous ASL (pCASL) to examine the structural and functional imaging data in schizophrenic patients, taking the regional cerebral gray matter volume into account. The subjects were 36 patients with schizophrenia and 42 healthy volunteers who underwent 3-tesla MRI, diffusion tensor imaging (DTI), and pCASL. We evaluated the gray matter volume imaging, DTI, and pCASL imaging data in a voxel-by-voxel statistical analysis. The schizophrenia patients showed reduced rCBF in the left prefrontal and bilateral occipital cortices compared to the healthy volunteers. There was a significant reduction of gray matter volume in the left inferior frontal cortex in the schizophrenia patients. With respect to the fractional anisotropy (FA) values in the DTI, there were significant FA reductions in the left superior temporal, left external capsule, and left inferior prefrontal regions in the patients compared to the controls.
Conclusion: Our pCASL study with partial volume effect correction together with volumetry and DTI data demonstrated hypoactivity in the left prefrontal area beyond structural abnormalities in schizophrenia patients. There were also hypofunction areas in bilateral occipital cortices, although structural abnormalities were not apparent.

1. Introduction

Schizophrenia is a complex disorder characterized by symptoms such as hallucinations, delusions, disorganized communication, poor planning, reduced motivation, and blunted affect. Structural brain abnormalities, such as ventricular enlargement, total brain volume deficits, and deficits in brain volume within the frontal, temporal, and parietal regions have been consistently reported in people with schizophrenia (reviewed in Shenton et al., 2001; Honea et al., 2005; Kanaan et al., 2005; Kubicki et al., 2007). Previous studies using nuclear medicine techniques such as single photon emission computed tomography (SPECT) showed significant reductions of regional cerebral blood flow (rCBF) in the frontal, parietal, and temporal regions of people with schizophrenia (Vita et al., 1995; Kanahara et al., 2009).

Arterial spin labeling (ASL) magnetic resonance imaging (MRI) is a novel noninvasive (i.e., non-radioactive) technique that can measure rCBF by taking advantage of arterial water as a freely diffusible tracer. A few studies have shown that ASL is useful to detect functional abnormalities of the brain in schizophrenic individuals (Horn et al., 2009; Scheef et al., 2010; Pinkham et al., 2011; Walther et al., 2011). Some of these studies showed the rCBF reduction in the frontal and parietal regions (Scheef et al., 2010; Pinkham et al., 2011; Walther et al., 2011), occipital region (Pinkham et al., 2011), and the temporal region and cingulum (Scheef et al., 2010; Walther et al., 2011); however, another study found no significant difference between patients and controls (Horn et al., 2009). Additionally, the limited spatial resolution of ASL images precludes exact rCBF measurements because the partial volume effects on ASL cause an underestimation of activity in small structures of the brain. Since many schizophrenia patients have altered brain structures as described above, their rCBF images are likely to be influenced by the partial volume effect. To our knowledge, however, no ASL study has thus far taken account of the partial volume effect.

In this study, we examined differences in rCBF between patients with schizophrenia and healthy controls by a recently developed method, pseudo-continuous ASL (pCASL). pCASL combines the advantages of pulsed ASL (PASL) and continuous ASL (CASL); PASL is less costly and CASL has a higher signal-to-noise ratio. Previously we demonstrated that pCASL could show the change of rCBF in multiple

* Corresponding author at: Department of Mental Disorder Research, National Institute of Neuroscience, National Center of Neurology and Psychiatry, 4-1-1, Ogawa-Higashi, Kodaira, Tokyo 187-8502, Japan. Tel.: +81 42 341 2712; fax: +81 42 346 2094.
E-mail address: ota@ncnp.go.jp (M. Ota).

0920-9964/$ – see front matter © 2014 Elsevier B.V. All rights reserved.
http://dx.doi.org/10.1016/j.schres.2014.01.035

sclerosis in a similar way as SPECT (Ota et al., 2013). Simultaneously, we also evaluated structural differences between the two groups by a three-dimensional volumetric acquisition of T1-weighted sequences and diffusion tensor imaging (DTI).

2. Materials and methods

2.1. Subjects

The subjects were 36 patients with schizophrenia and 42 age- and gender-matched healthy subjects. A consensus diagnosis by at least two psychiatrists was made according to the Diagnostic and Statistical Manual of Mental Disorders, 4th ed. (DSM-IV) criteria (American Psychiatric Association, 1994), on the basis of unstructured interviews and information from medical records. Twenty-one of the 36 patients were inpatients and were admitted to an acute psychiatric ward of the National Center of Neurology and Psychiatry Hospital, Japan. Thirty-four of the 36 patients were chronic cases, and the remaining two patients were experiencing first-episode schizophrenia. The psychopathological state of all of the schizophrenic patients was assessed with the Positive and Negative Syndrome Scale (PANSS) (Kay et al., 1987).

Controls were recruited from the community through local magazine advertisements and our website announcement. These participants were interviewed for enrollment by a research psychiatrist using the Japanese version of the Mini-International Neuropsychiatric Interview (Sheehan et al., 1998; Otsubo et al., 2005). Participants were excluded if they had a prior medical history of central nervous system disease or severe head injury, or if they met the criteria for substance abuse or dependence. Those individuals who demonstrated a history of psychiatric illness or contact with psychiatric services were excluded from the control group. Daily doses of antipsychotics, including depot antipsychotics, were converted to chlorpromazine equivalents using published guidelines (American Psychiatric Association, 1997; Inagaki et al., 1999).

After the study was explained to each participant, his or her written informed consent was obtained for participation in the study. This study was approved by the ethics committee of the National Center of Neurology and Psychiatry, Japan.

2.2. MRI data acquisition and processing

Imaging was performed on a 3-tesla MR system (Philips Medical Systems, Best, The Netherlands). High spatial resolution, 3-dimensional (3D) T1-weighted images were used for the morphometric study. 3D T1-weighted images were acquired in the sagittal plane (repetition time [TR]/echo time [TE], 7.18/3.46; flip angle, 10°; effective section thickness, 0.6 mm; slab thickness, 180 mm; matrix, 384 × 384; field of view [FOV], 261 × 261 mm; number of signals acquired, 1, yielding 300 contiguous slices through the brain.

DTI was performed in the axial plane (TR/TE, 5760/62 ms; matrix, 80 × 80; FOV, 240 × 240 mm; 60 continuous transverse slices; slice thickness 3 mm with no interslice gap). To enhance the signal-to-noise ratio, acquisition was performed two times. Diffusion was measured along 15 non-collinear directions using a diffusion-weighted factor *b* in each direction for 1000 s/mm2, and one image was acquired without using any diffusion gradient. The imaging parameters for all of the pCASL experiments were identical: single-shot gradient-echo echo planar imaging (EPI) in combination with parallel imaging imaging (SENSE factor 2.0), TR = 4000 ms, TE = 12 ms, matrix = 64 × 64, FOV = 240 × 240, voxel size = 3.75 × 3.75 mm, 20 slices acquired in ascending order, slice thickness = 7 mm, 1-mm gap between slices, labeling duration = 1650 ms, post-spin labeling delay = 1520 ms, time interval between consecutive slice acquisitions = 32.0 ms, RF duration = 0.5 ms, pause between RF pulses = 0.5 ms, labeling pulse flip angle = 18°, bandwidth = 3.3 kHz/pixel, echo train length = 35. Thirty-two pairs of control/label images were acquired and averaged. The scan duration was 4 min and 24 s. For measurement of the magnetization of arterial blood and also for segmentation purposes, an EPI M0 image was obtained separately with the same geometry and the same imaging parameters as the pCASL without labeling.

2.3. Postprocessing of the ASL data

Because the pCASL and M0 images were acquired separately, the image signal intensities of both were corrected for data scaling. Corrected data were transferred to a workstation and analyzed by using ASLtbx software (Wang et al., 2008) running on statistical parametric mapping 5 (SPM5). For the rCBF calculations, we added the attenuation correction for the transversal relaxation rate of gray matter to the original equation. Details of this process are described elsewhere (Ota et al., 2013). The parameters used in the present study were: longitudinal relaxation time of blood = 1664 ms (Lu et al., 2004), labeling efficiency = 0.85 (Aslan et al., 2010), transversal relaxation time of gray matter (assumed to be 44.2 ms; Cavuşoğlu et al., 2009), and blood/tissue water partition coefficient = 0.9 g/ml (Wang et al., 2005).

The mean rCBF image derived by using the ASLtbx software contained some patchy noise, and thus we used a median filter (a nonlinear digital filtering technique). In median filtering, the neighboring pixels are ranked according to their intensity, and the median value becomes the new value for the central pixel. Since the slice gap that we used was somewhat large, simple 2D median filtering (3 voxels × 3 voxels) was used. To evaluate rCBF on a voxel-by-voxel basis, we normalized the mean rCBF images to the standard space. First, each individual 3D-T1 image was coregistered and resliced to its own M0 image. Next, the coregistered 3D-T1 image was normalized to the "avg152T1" image regarded as the anatomically standard image. Finally, the transformation matrix was applied to the mean rCBF images treated with the median filter. The spatially normalized images were resliced with a final voxel size of approx. 4 × 4 × 8 mm. Each map was then spatially smoothed with a 4-mm full-width at half-maximum Gaussian kernel in order to decrease spatial noise and compensate for the inexactitude of normalization.

2.4. Diffeomorphic anatomical registration using an exponentiated lie algebra (DARTEL) analysis

A preprocessing step of voxel based morphometry (VBM) in SPM was improved with the DARTEL (diffeomorphic anatomical registration using exponentiated lie) registration method (Ashburner, 2007). Calculations and image matrix manipulations were performed by using SPM8 working on a Matlab 7.0 (Math Works, Natick, MA, USA). The brain images were segmented, normalized, and modulated by using a set of group-specific templates. The gray matter probability values were then smoothed by using a 12-mm full-width at half-maximum Gaussian kernel.

2.5. Tract-based spatial statistics (TBSS) analysis

We evaluated the fractional anisotropy (FA) images by the processing technique known as tract-based spatial statistics (TBSS) analysis (Smith et al., 2006). TBSS is available as part of the FSL 4.1 software package (Smith et al., 2004). TBSS projects each subject's aligned FA image to the FMRIB58_FA template, which is supplied with FSL, onto the binary mask called the "skeleton image" derived from the mean FA image limited the FA value to >0.2. This results in skeletonized FA data. It is this file that is used for the voxelwise statistics.

Please cite this article as: Ota, M., et al., Pseudo-continuous arterial spin labeling MRI study of schizophrenic patients, Schizophr. Res. (2014), http://dx.doi.org/10.1016/j.schres.2014.01.035